journal of the international meteor organization

WGN

47:3
june 2019

Meteorite-dropping fireball over Poland on 2018 Oct 5/6
Perseid fireball of 2018 Aug 13 seen by video, photo, and radar
May-June IMO video meteors
Meteor reports in The Astronomer magazine - part IV

ISSN 1016-3115

WGN Vol. 47, No. 3, June 2019, pp. 75 – 106

Fireballs

Preliminary results

History

Front cover photo

Brilliant fireball captured on 2019 February 26 at $06^{h}14^{m}$ UT, from Vilaflor, Santa Cruz de Tenerife, Canary Islands. Photo courtesy: Hermann Koberger.

Writing for WGN

This Journal welcomes papers submitted for publication. All papers are reviewed for scientific content, and edited for English and style. Instructions for authors can be found in WGN **45:1**, 1–5, and at `http://www.imo.net/docs/writingforwgn.pdf` .

Copyright

Legal address

International Meteor Organization, Jozef Mattheessensstraat 60, 2540 Hove, Belgium.

Fireballs

PF061018 Bukienka – meteorite dropping fireball

A. Olech[1], *P. Żołądek*[2], *M. Wiśniewski*[2], *H. Krygiel*[2], *M. Kwinta*[2], *M. Myszkiewicz*[2], *P. Nowak*[2], *K. Polak*[2], *K. Polakowski*[2], *A. Raj*[2], *M. Szlagor*[2], *J. Twardowski*[2], *and Z. Tymiński*[3]

On the night 2018 October 5/6, at $00^h26^m51^s$ UT, the fireball with maximum absolute magnitude of -9.7 ± 0.5 appeared over southern Poland. The precise orbit and atmospheric trajectory of the event are presented, based on the data collected by ten video stations of the *Polish Fireball Network (PFN)*. The PF061018 Bukienka fireball entered the Earth's atmosphere with the velocity of 18.2 ± 0.2 km/s and started to shine at a height of 86.0 ± 0.1 km. Clear deceleration started after the first five seconds of the flight, and the terminal velocity of the meteor was only 4.9 ± 0.2 km/s at a height of 30.8 ± 0.1 km. Such a low value of the terminal velocity indicates that ablation process stopped and small fragments with the total mass of around $50 - 150$ g could survive the atmospheric passage and cause fall of the meteorites. The predicted area of possible meteorite impact is computed and it is located between Taraska and Kotuszów villages less than 20 km from Piotrków Trybunalski town.

Received 2019 April 26

1 Introduction

The *Polish Fireball Network (PFN)* is a project established in 2004, whose main goal is to constant monitoring the sky over Poland in order to detect bright fireballs occurring over the whole territory of the country (Olech et al., 2006; Wiśniewski et al., 2017). It is run by amateur astronomers associated in the *Comets and Meteors Workshop (CMW)* and coordinated by astronomers from the Copernicus Astronomical Center in Warsaw, Poland. Today there are over 35 fireball stations belonging to *PFN* that operate during each clear night. In total over 70 sensitive CCTV cameras with fast and wide angle lenses are used.

In this paper we report an analysis of the multistation observation of the PF061018 Bukienka fireball made by cameras of the *Polish Fireball Network*. The trajectory, orbit and possible area of meteorite fall are calculated.

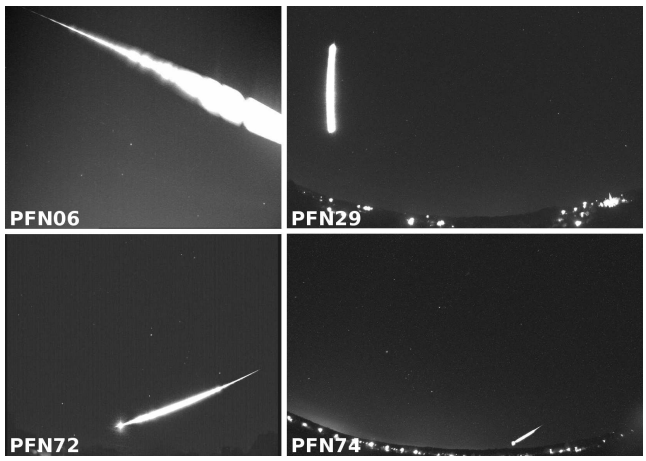

Figure 1 – The mosaic of video images of the PF061018 Bukienka fireball as seen by four PFN stations.

2 Observations and data reduction

Due to extremely good weather conditions the PF061018 Bukienka fireball was observed by ten *PFN* video stations quite uniformly distributed over the whole country (see Figure 1 showing the mosaic of images from four our stations). Our stations are listed in Table 1 together with their respective coordinates and equipment used for recording the fireball. Additionally, the meteor was recorded using the allsky weather station at Mt. Suhora Astronomical Observatory.

The data from our stations used for calculations, after a preliminary conversion, were additionally reduced astrometricaly by the UFO Analyzer application (SonotaCo, 2009). Initially, only automatic data were taken into account but during later processing it became obvious that significant overexposures, presence of the wake and a possible fragmentation after the flare caused substantial errors in position of the points of the phenomenon calculation. To improve the measurement precision, the bolide's position was determined with the help of an UFOAnalyzer astrometric solution using a manual centroid measurement. Moreover, in cases where saturated areas did not allow the precise determination of the centroid, the wake of the fireball was used for measuring the position.

Due to the very low angular velocity of the event many of our stations captured the fireball path only partially. The most complete recordings come from PFN72 Koźmin Wielkopolski and PFN24 Gniewowo stations, where whole path of the fireball was captured, and these data were mostly used for velocity determination. The highest precision astrometric solution comes from PFN29 Klecza Dolna station working in Full HD resolution. In spite of significant saturation, presence of the clear wake allowed to determine the path of the fireball with high precision.

[1]Copernicus Astronomical Center, Polish Academy of Sciences, ul. Bartycka 18, 00-716 Warszawa, Poland.
[2]Comets and Meteors Workshop, ul. Bartycka 18, 00-716 Warszawa, Poland.
[3]Narodowe Centrum Badań Jądrowych, Ośrodek Radioizotopów POLATOM, ul. Sołtana 7, 05-400 Otwock, Poland.

IMO bibcode WGN-473-olech-bukienka
NASA-ADS bibcode 2019JIMO...47...75O

Table 1 – Basic data on the PFN stations which recorded the fireball.

Code	Site	Longitude [°]	Latitude [°]	Elev. [m]	Resolution [pix]	FoV [°]
PFN06	Kraków	19.9424 E	50.0216 N	250	786 × 568	70
PFN24	Gniewowo	18.3042 E	54.5779 N	130	1920 × 1200	100
PFN29	Klecza Dolna	19.5374 E	49.8730 N	285	1920 × 1200	100
PFN40	Otwock	21.2494 E	52.1078 N	100	786 × 568	70
PFN41	Twardogóra	17.4589 E	51.3702 N	178	786 × 568	70
PFN43	Siedlce	22.2925 E	52.2147 N	150	1920 × 1200	100
PFN51	Zelów	19.2232 E	51.4698 N	200	786 × 568	70
PFN60	Bystra	19.1892 E	49.6215 N	444	786 × 568	70
PFN63	Starowa Góra	19.4795 E	51.6864 N	189	1920 × 1200	180
PFN72	Koźmin Wlkp.	17.4548 E	51.8283 N	139	786 × 568	70
OA UP	Suhora	20.0675 E	49.5691 N	1009	640 × 480	180

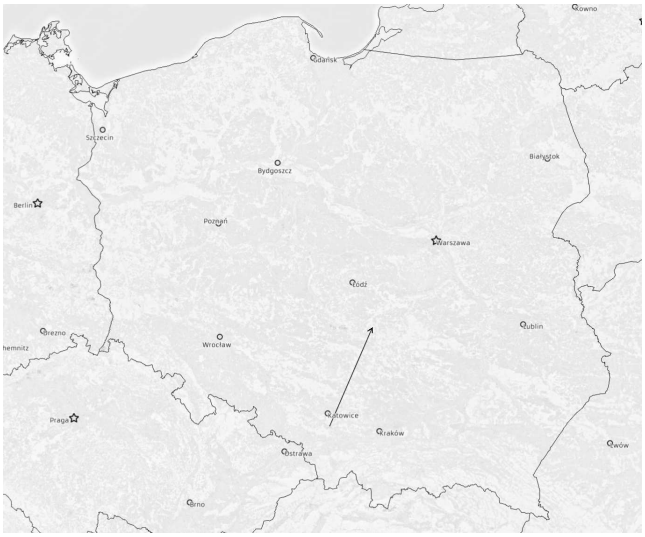

Figure 2 – The luminous trajectory of the PF061018 Bukienka fireball over Poland.

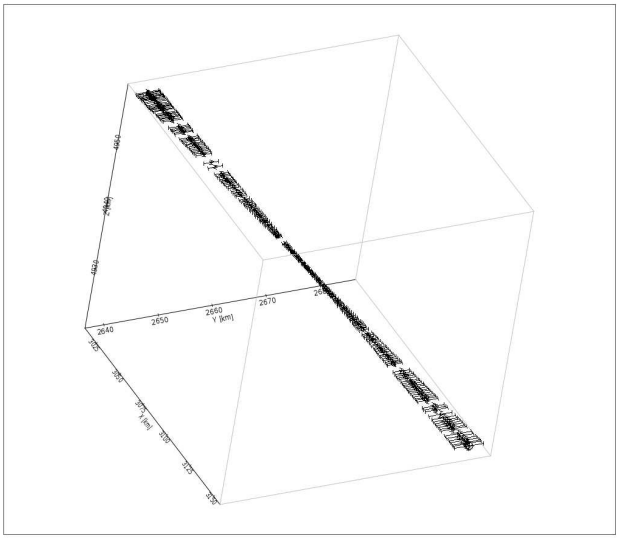

Figure 3 – Positional X,Y,Z errors along the fireball trajectory. Error bars enlarged ten times for better clarity. Geocentric Cartesian coordinate system was used.

The image from the allsky station at Suhora Observatory has too low resolution for using it for astrometry, but it was useful for absolute magnitude determination.

The trajectory and orbit of the fireball were computed using the PyFN software (Zoladek, 2012). PyFN is written in Python with usage of the SciPy module and the CSPICE library. For the purpose of trajectory and orbit computation, it uses the plane intersection method described by Ceplecha (1987). Moreover, PyFN accepts data in both MetRec (Molau, 1999) and UFOAnalyzer (SonotaCo, 2009) formats and allows a semi-automatic search for double-station meteors.

3 Results

3.1 Trajectory of the fireball

The Bukienka fireball moved almost directly from south-west to north-east following a moderately steep trajectory having a total length of almost 205 km. The beginning of the bolide was located over Tychy at the height of 86.0 ± 0.1 km. During next seconds the bolide traveled north-east and flew 41.5 ± 0.1 kilometers over Bukienka village (east of Radom), reaching its maximum brightness there. The terminal point of the trajectory was situated at the height of 30.8 ± 0.1 km over the place located 13 km south of Sulejów. The exact values of positional errors along and across the trajectory path at its end are respectively 88 and 199 meters.

The trajectory of the PF061018 fireball is shown in Figures 2 and 3, and all important parameters are summarized in Table 2.

According to the visual observers, the fireball fragmented into five parts. The PFN cameras show fragmentation just after the maximum brightness. The first fragment is seen at $t = 7.8$ s, the second one at $t = 8.0$ s, and the third one at $t = 8.28$ s. The backward prolongation of the paths of the observed fragments indicates that fragmentation occurred no later than at $t = 7.52$ s. For comparison, the maximum brightness is observed at $t = 6.42$ s but it is wide and ends finally around $t = 7.2$ s.

3.2 Velocity

Based on our observations the velocity of the object was estimated for different points of its trajectory. In the initial part of the flight the velocity did not change in a noticeable way and was almost constant at a value

Table 2 – Characteristics of the PF061018 Bukienka fireball.

2018 October 6, T = $00^h26^m51^s \pm 1.0^s$ UT			
Atmospheric trajectory data			
	Beginning	**Max. light**	**Terminal**
Vel. [km/s]	18.2 ± 0.2	15.6 ± 0.2	4.9 ± 0.2
Height [km]	86.0 ± 0.1	41.52 ± 0.05	30.8 ± 0.05
Long. [°E]	19.060 ± 0.002	19.665 ± 0.002	19.816 ± 0.003
Lat. [°N]	50.120 ± 0.003	51.0145 ± 0.0006	51.2375 ± 0.0008
Abs. magn.	0.4 ± 0.5	-9.7 ± 0.5	0.8 ± 0.5
Slope [°]	22.6 ± 0.2	21.6 ± 0.2	21.3 ± 0.2
Duration		9.2 s	
Lenght		204.6 ± 0.6 km	
Radiant data (J2000.0)			
	Observed	**Geocentric**	**Heliocentric**
RA [°]	17.6 ± 0.2	13.6 ± 0.2	—
Decl. [°]	-14.27 ± 0.02	-22.88 ± 0.2	—
Vel. [km/s]	18.2 ± 0.2	14.5 ± 0.2	35.0 ± 0.2

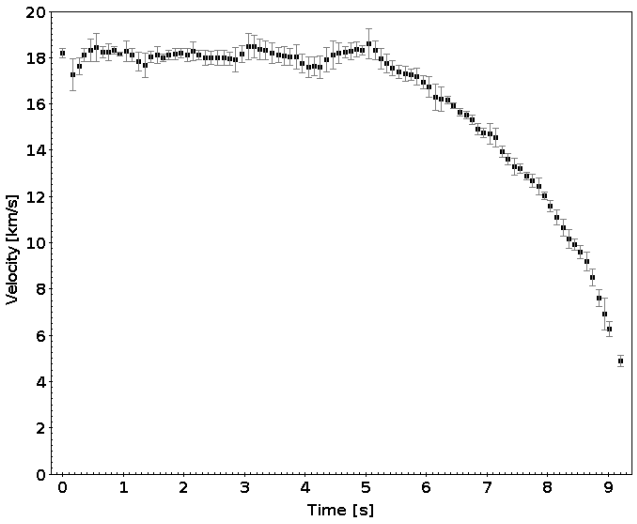

Figure 4 – The evolution of the velocity of the PF061018 Bukienka fireball.

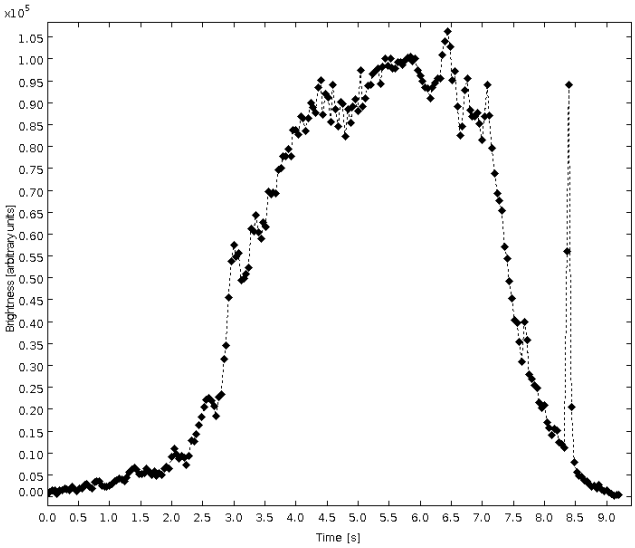

Figure 5 – The light curve of the PF061018 Bukienka fireball.

of around 18 km/s. After the fifth second of the flight the velocity decrease became clearly visible, with final deceleration as high as 8200 ± 800 m/s^2. At the end of the luminous trajectory the velocity of the fireball was only 4.9 ± 0.2 km/s (see Figure 4).

3.3 Brightness

The light curve of the PF061018 Bukienka fireball is shown in Figure 5. The brightness of the meteor increases slowly during first 2.5 seconds of flight. After that moment one can see rapid increase of brightness which ends with clear plateau phase lasting about three seconds. During this plateau the maximum brightness with -9.7 ± 0.5 absolute magnitude is reached.

After 8 seconds of flight the fireball shows luminous flash with maximum brightness of around -8 mag lasting only 0.12 seconds. The meteor survives this flash and continues its flight for another one second while slowly fading.

3.4 Dark flight and a possible fall of the meteorite

With the terminal speed 4.9 km/s and the height slightly above 30 km there is a possible meteorite fall from the main fragment of the body. Using the terminal point parameters, the darkflight calculations been performed using method described by Ceplecha (1987). Using the terminal point parameters and its uncertainties a few hundreds of clones has been created with slightly modified input parameters, from the results of such calculations mean results and its uncertainties has been determined. The GFS model wind and pressure data were used for darkflight calculations.

Possible meteorite is small, with mass of 100 ± 50 grams. After the 500 seconds of darkflight the meteorite impacted the Earth's surface with the speed close to 30 m/s. There is a large uncertainty of meteorite impact point caused by high altitude winds. The area of highest probability is 6 kilometers long and 300 m wide. The center of this area is located between villages Taraska and Kotuszów, 6 kilometers south-east of Sule-

Table 3 – Orbital elements of the PF1061018 Bukienka fireball.

	$1/a$ [1/AU]	e	q [AU]	ω [deg]	Ω [deg]	i [deg]
PF061018	0.618(4)	0.510(4)	0.793(2)	67.2(4)	19.45(3)	11.36(6)

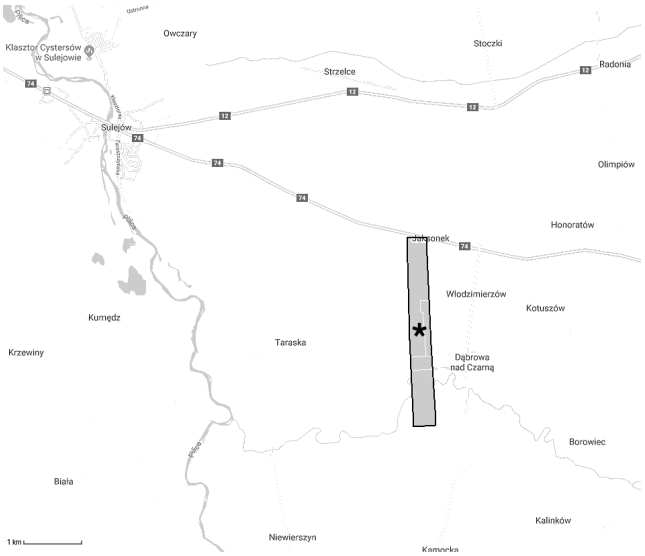

Figure 6 – The computed impact area of meteorite caused by the PF061018 Bukienka fireball.

jów (see Figure 6). It is likely that only one significant piece of meteorite felt on the ground, the other observed fragments terminated its luminous flight at the height larger than 34 km and its terminal mass is neglectable. The meteorite has not been recovered yet.

3.5 Orbit

Based on the observational data we were able to determine the radiant of the PF1061018 Bukienka, its geocentric velocity and orbital parameters of the meteoroid which entered the Earth's atmosphere. The orbital parameters of the meteoroid which caused the fireball are listed in Table 3.

The orbit is classic asteroid orbit with slight inclination to the ecliptic ($i = 11$ deg) with semimajor axis equal to 1.61 AU. There are no similarities of the determined orbit to the orbits of known NEOs and comets.

Acknowledgments

This project was supported by the work of amateur astronomers – members of the Comets and Meteors Workshop.

References

Ceplecha Z. (1987). "Geometric, dynamic, orbital and photometric data on meteoroids from photographic fireball networks". *Bulletin of the Astronomical Institutes of Czechoslovakia*, **38**, 222–234.

Molau S. (1999). "The meteor detection software MetRec". In Baggaley W. J. and Porubcan V., editors, *Meteoroids 1998. Proceedings of the International Conference held at Tatranska Lomnica, Slovakia, August 17-21, 1998.* Astronomical Institute of the Slovak Academy of Sciences, pages 131–134.

Olech A., Zoladek P., Wisniewski M., Krasnowski M., Kwinta M., Fajfer T., Fietkiewicz K., Dorosz D., Kowalski L., Olejnik J., Mularczyk K., and Zloczewski K. (2006). "Polish Fireball Network". In Bastiaens L., Verbert J., Wislez J.-M., and Verbeeck C., editors, *Proceedings of the International Meteor Conference, 24th IMC, Oostmalle, Belgium, 2005.* pages 53–62.

SonotaCo (2009). "A meteor shower catalog based on video observations in 2007-2008". *WGN, Journal of the IMO*, **37**, 55–62.

Wiśniewski M., Żołądek P., Olech A., Tyminski Z., Maciejewski M., Fietkiewicz K., Rudawska R., Gozdalski M., Gawroński M. P., Suchodolski T., Myszkiewicz M., Stolarz M., and Polakowski K. (2017). "Current status of Polish Fireball Network". *Planetary and Space Science*, **143**, 12–20.

Zoladek P. (2012). "PyFN - multipurpose meteor software". In Gyssens M. and Roggemans P., editors, *Proceedings of the International Meteor Conference, 30th IMC, Sibiu, Romania, 2011.* pages 53–55.

Handling Editor: Javor Kac
This paper has been typeset from a LaTeX file prepared by the authors.

3414-2018: A Perseid fireball showing exceptional light effects, observed by video, photo and radio

Peter C. Slansky[1] *and Bernd Gaehrken*[2]

This article is about the observation of 3414-2018, a 2018 Perseid fireball, with video, photo and radio in parallel from three different observing sites so that the trajectory could be calculated. The fireball showed exceptional light effects, including a very bright terminal flash with a radius of up to 4 km, a persistent train, a green afterglow and a diffuse, widespread bluish sky glow with a radius of more than 120 km, persisting for up to half a second. These observations were possible only by the use of two very high sensitive cameras in video mode with full HD resolution in colour independently.

Received 2019 February 9

1 Introduction

Fireball patrol has become popular. Some fireball events have been reported by more than a thousand people. So far, the all-time No. 1 on the IMO fireball website is event 4299-2017 (IMO, 2017) over Frankfurt, Germany, reported by 2046 observers from eight European countries, followed by event 3638-2014 (IMO, 2014) over Pittsfield, Massachusetts, USA, reported by 1547 observers from the US and Canada. Other fireballs gain celebrity status when new observation techniques facilitate new information about their physical nature. Hence, a 2001 Leonid became famous because it was observed with an intensified high speed video camera at 1000 frames per second, revealing an axe-shaped shock halo of a meteor head for the first time (Jenniskens & Stenbaek-Nielsen, 2004). EN120812, a −9 mag 2012 Perseid fireball, became the "haul" of no less than 17 professional meteor cameras in Czechia (Spurný et al., 2014), revealing a record breaking entering altitude of 170 km and a lot of other detailed information. Both observations induced a lot of scientific papers including new models of the physical principles of meteor light distribution. Also in this article, there will be further references to these events.

The main character of this article is a Perseid fireball that lighted up on 2018 August 13 at 01^h51^m UT over Ingolstadt, Southern Germany (IMO, 2018). To the knowledge of the authors only two visual observations were reported (not by the authors, unfortunately). But it was recorded by amateurs (alone) with three different observation techniques, independently: Photography, video and radio – still a quite rare parallelism. After the report to the IMO by the authors this fireball gained IMO code 3414-2018. By a joint examination together with two other German amateurs, Juergen Michelberger and Reinhardt Wurzel, who had observed it as well, 3414-2018 turned out to be an outstanding specimen of the rich family of the Perseids: It entered the atmosphere at a height of 159 km, produced a terminal flash of −7 mag (according to Wurzel (2019)) at a height of 82 km and expired at a height of 77 km, leaving behind a persistent train that was visible for about 3 minutes and more than 7 minutes on a photo series. The terminal flash was accompanied (respectively followed) by a strong green afterglow with a comparably sharp outline with a radius of up to 4 km. Even more astonishing, the terminal flash and the green afterglow were not just reflected by the atmosphere but were accompanied (respectively followed) by a widespread bluish sky glow that persisted up to 480 ms, recorded by two cameras independently, up to a distance of 122 km from the point of the terminal flash. The areal dimensions of the light distribution of 3414-2018 were so exceptional that the authors made a line of technical tests to rule out camera or lens artefacts, what the tests definitively did. The meteor was also observed by a radio amateur from Dessau, Middle Germany, who had his antenna pointed to the GRAVES radar in France. The train echo lasted 43 s and showed a significant Doppler shift. So, further examination of 3414-2018 seems to be highly valuable.

2 Observation

The first report of this fireball to the IMO came from the authors. We had observed the 2018 Perseids in the first night on August 11/12 from Oberes Sudelfeld, Bavarian Alpine Mountains, 1420 m altitude. Due to the weather forecast for the second night on August 12/13, we moved to Geigersau, Upper Bavaria, 930 m altitude (47.72701° N / 11.02595° E). At 03^h51^m CEST (= 01^h51^m UT) we were both busy with a technical camera test. So, we missed the sight of our brightest 2018 Perseid. We only saw the reflection of its terminal flash on the ground like a flash light. Luckily, it turned out that this fireball had been covered by the fields of the two high sensitivity digital cameras Sony α7S running in video mode (Figure 1) and also, for the most part, by a photo camera Canon EOS M (Figure 3). The video of 3414-2018 was presented by Peter C. Slansky on the IMC 2018 in Pezinok, Slovakia (Slansky, 2019).

The Sonys had recorded more than 500 meteors in the two Perseids nights, but when the videos were analyzed, the fireball at 01^h51^m UT caught our special attention because of its exceptional light effects (Figure 2). Although both authors had missed the fireball visually, we reported it to the IMO and uploaded our videos and photos. By this "our" fireball became 3414-2018 – ready to be shared with the meteor observers' community.

Soon we were happy to hear from Juergen Michelberger and Reinhardt Wurzel who had observed 3414-

[1]Email: slansky@mnet-online.de
[2]Email: bgaehrken@web.de

IMO bibcode WGN-473-slansky-fireball
NASA-ADS bibcode 2019JIMO...47...79S

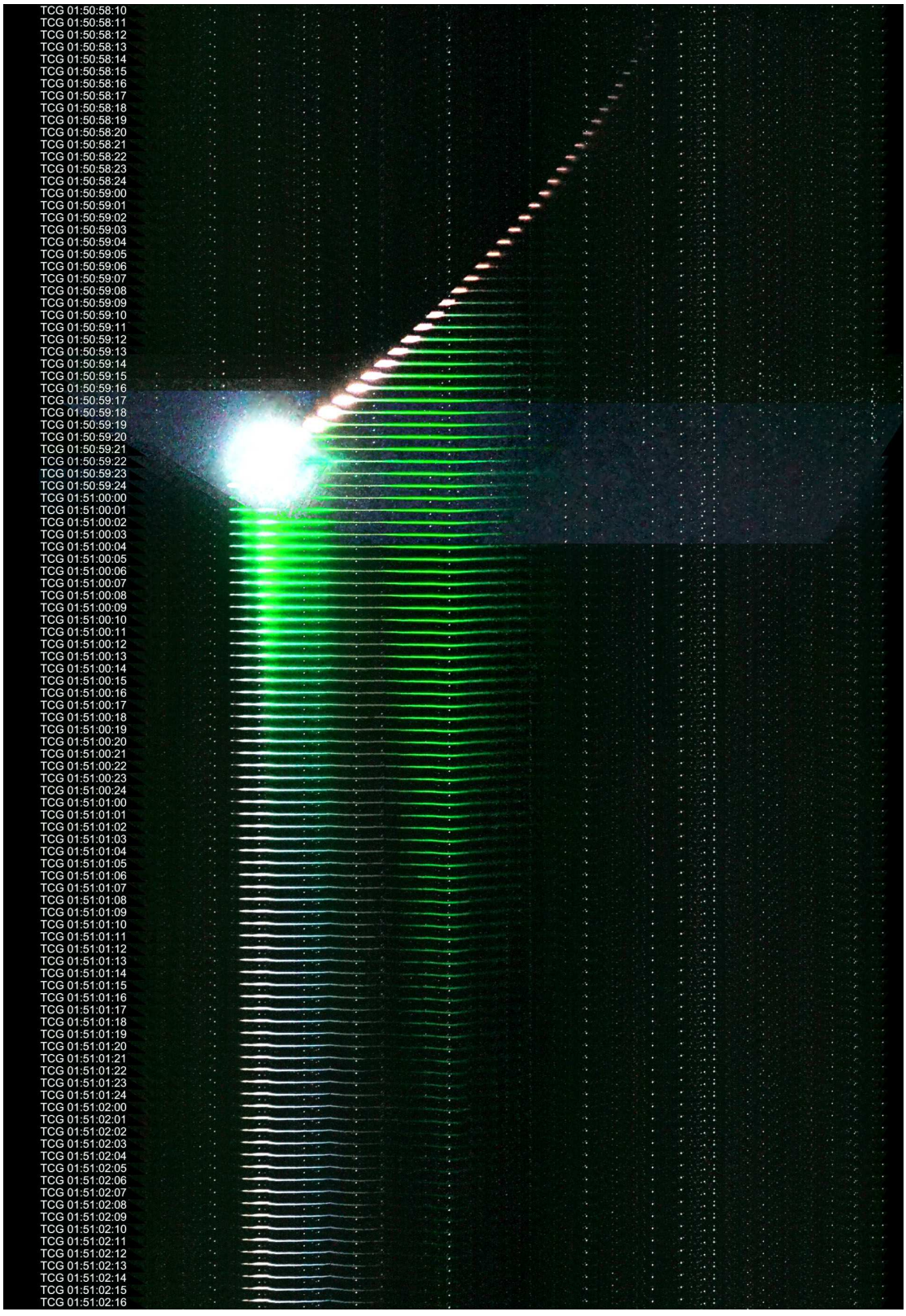

Figure 1 – Sequence analysis of fireball 3414-2018 on 2018 August 13, $01^{h}51^{m}$ UT, observed by Peter C. Slansky at Geigersau, Upper Bavaria, Germany, together with Bernd Gaehrken. The original video was shot with two Sony α7S cameras at 25 fps with $t = 1/25$ s and ISO 409 000, equipped with two Canon FD 1.4/50mm lenses at $F = 1.4$. The meteor appeared in the field of view of camera 1, pointing to Camelopardalis in the image center, from right to left. Then it changed to the field of view of camera 2, pointing to Ursa Minor, where it ended in a terminal flash. The embedded real time code (UT) indicates the temporal development in hours:minutes:seconds:frames. The time of a radio clock had been transferred manually to the time code setting of the cameras with an estimated precision of about 250 ms. The images were rotated clockwise so that the meteor proceeds exactly from right to left in the composite. Hence, in this composite every vertical step from top to bottom represents a temporal step of 1/25 s = 40 ms. In every image a line of stars appears. To show the dimensions of the – strongly overexposed – terminal flash five frames around frame 01:50:59:22 are shown as an overlay on the rest of the sequence analysis (note the additional stars appearing only in these five wider stripes).

Figure 2 – The terminal flash of 3414-2018 in a compositing of two single video frames of camera 1 (right) and camera 2 (left). The image center of camera 1 pointed to Camelopardalis, the image center of camera 2 to Ursa Minor. The border between the two camera fields is visible on the beginning of the green train. The bright star slightly right from the image center is Polaris. It has "wings" due to artefacts of the lens (curvature of field, astigmatism and coma). On the right and upper side of the white clipped area of the terminal flash block-shaped data compression artefacts can be seen. They are caused by the recording codec of the camera. The widespread bluish sky glow that appears in the fields of view of both cameras is no artefact. It will be examined in detail in Section 4.6.

Figure 3 – Persistent train of 3414-2018 photographed by Bernd Gaehrken in a series from Geigersau with a Canon EOS M at ISO 3200 with 15 s integration time with Canon 2.8/50mm lens set to $F = 2.8$ (Gaehrken, 2018). The persistent train was warped by wind. Please also note the changes in colour. It will be described in detail in Section 4.7.

2018 visually and had photographed it, too (Figure 4). Their observing site had been Horní Vltavice, Czechia, at 822 m altitude (48.952° N /13.765° E). By a lucky coincidence, our observing directions were rectangular: we, "team Geigersau", had pointed our cameras to the North, catching the fireball in Ursa Minor, "team Horní Vltavice" had pointed their camera (and their eyes) to the West with the fireball appearing in Sagitta/Aquila. With the video from Geigersau and the photo from Horní Vltavice, Juergen Michelberger calculated the trajectory. Reinhardt Wurzel provided additional information about the atmosphere, while the authors started a qualitative and quantitative analysis of the videos and photos.

Team Geigersau operated two Sony α7S equipped with Canon FD 1.4/50 mm lenses set to $F = 1.4$. According to earlier experiences (Slansky, 2016), the cameras were run with 25 frames per second with an exposure time of 1/25 s at the maximum sensitivity ISO 409 000. In earlier tests this camera-lens combination – with the lens stopped down to $F = 2.0$ – had achieved a stellar limiting magnitude of 8.7 mag (Slan-

Figure 4 – 3414-2018 photographed by Juergen Michelberger from Horní Vltavice, Czechia, together with Reinhardt Wurzel, with a Canon EOS 700D at ISO 1600 and 60 s exposure time with a Tamron 2.8/17-50mm zoom lens at $f = 17$ mm and $F = 2.8$. The exact exposure interval was from $01^h50^m32^s$ to $01^h51^m32^s$ UT ± 1 s. The camera was pointing to the West, so the fireball appears in the constellations Sagitta/Aquila. Unfortunately, there was some dew on the front lens.

sky, 2018a). Both cameras were mounted on a parallactic mounting with the long axis of the fields orientated towards the radiant in an angle so that Polaris was in the overlap of both camera fields on the short axis. A focal length of 50 mm provided a field of view of 39.0° × 22.7° at an aspect ratio 16:9 on the Sony's sensors. With this camera-lens combination the angular resolution was 1.24 arcminutes per pixel, corresponding to 48.45 pixels per degree.[a] The recording was done in full HD resolution 1920 × 1080 pixels via internal recording with XAVC S, 50 Mbit/s, 8 bit per channel.

Additionally, a Canon EOS M photo camera was mounted on another parallactic mounting. It was equipped with a Canon 2.8/50mm lens at $F = 2.8$. This camera was operated in a series with an exposure time of 15 s at ISO 3200. The fireball flew through the camera's field of view with the terminal flash outside but the biggest part of the persistent train was captured for seven minutes until the photo series was interrupted by technical reasons.

[a]This is an average value; according to the laws of perspective the angular resolution varies from the center of the image to the periphery.

Team Horní Vltavice used a Canon EOS 700D on a parallactic mounting with a Tamron zoom lens 2.8/17-50mm set to $f = 17$ mm and $F = 2.8$. The field of view was 47.3° × 66.5° at a resolution of 3456 × 5184 pixels. The camera was set to ISO 1600 with 60 s exposure time in a series. The exact exposure interval was from $01^h50^m32^s$ to $01^h51^m32^s$ UT ± 1 s. Unfortunately, there was some dew on the front lens. But the image was still usable. By a lucky coincidence, the cameras of team Geigersau and team Horní Vltavice were crossing their optical axis' at an angle of nearly 90° and the meteor crossed them at an angle of nearly 45° resulting in ideal geometrical conditions for the calculation of the trajectory.

3 Trajectory

Due to the differences in exposure the meteor head became visible in the video from Geigersau much earlier than in the photo from Horní Vltavice, as can be seen in Figure 6. According to this, Juergen Michelberger calculated the trajectory along four points:

- Point A: Meteor becomes visible in the video of Peter C. Slansky with a Sony α7S from Geigersau
- Point B: Meteor becomes visible in the photo of Juergen Michelberger with a Canon 700D from Horní Vltavice
- Point C: Terminal flash
- Point D: Expiration of the meteor.

Point D could be detected clearly in the photo as well as in the video. Due to the movement of the meteor, Point C had to be calculated from the centroid of the overexposed area of the terminal flash in both the photo and the respective frame of the video.

The meteor flight between point A and D was recorded over 39 video frames = 1560 ms. But the starting point A had to be interpolated between two video frames. So, the real duration of the meteor flight was

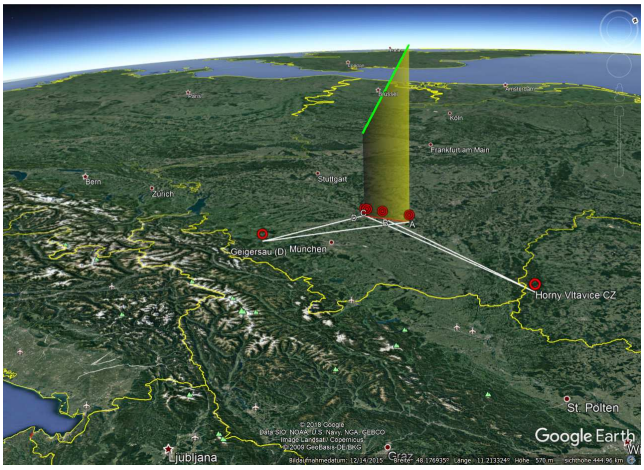

Figure 5 – Trajectory of 3414-2018 (green) with points A, B, C and D projected to the ground (red) and the projected viewing angles (white) from the two observation sites (red circles).

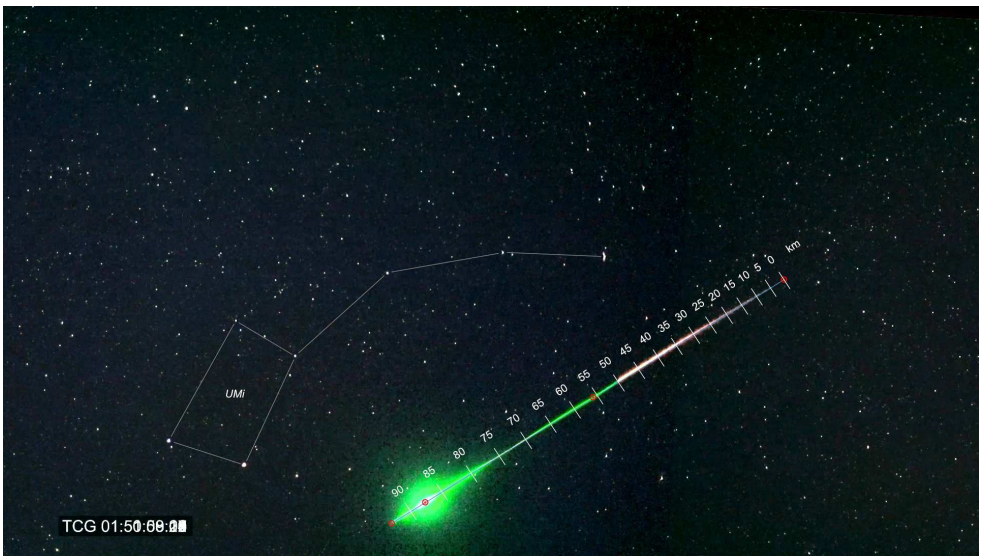

Figure 6 – Trajectory of 3414-2018 in the video from Geigersau with points A, B, C and D (red) and with the real length in km starting from point A (= 0 km). The entry point A indicates where the meteor became visible. It lies inside the integration time of 40 ms of video frame 01:50:58:11 UT [hh:mm:ss:ff].

38.3 frames = 1532 ms. In this time the meteor traveled a distance of 92.9 km. This means an average geocentric speed v_m = 60.6 km/s. It has to be taken into account, that the duration of half a video frame (= 20 ms) causes a difference in speed of 0.8 km/s. Closer examination revealed a speed between point A and B v_{AB} = 61.9 km/s and a speed between point B and D v_{BD} = 58.9 km/s. An amount of 0.11 km/s goes back to earth rotation. Hence, 3414-2018 was slightly faster than the literature speed values for Perseids ranging from 59 km/s (Rendtel, 2017) to 60 km/s (Hughes, 1995). The speed distribution of 3414-2018 between entry, terminal flash and expiration matches well with the 2012 Perseid fireball observed by Spurný et al. (2014).

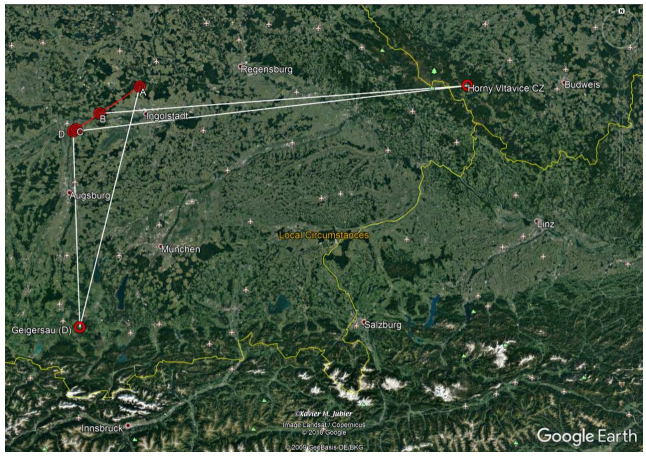

Figure 7 – Trajectory of 3414-2018 projected onto the ground (red). Note, that the fireball was recorded by the video camera from Geigersau via the angle A-D but by the photo camera from Horní Vltavice via the sharper angle B-D (both white).

4 Light distribution

4.1 Meteor head

According to Figure 1 the meteor head becomes visible in the video at frame 01:50:58:12 at an altitude of 158.6 km. The average motion blur of the meteor in each video frame is about 21 pixels. Due to the laws of perspective, the angular velocity of the meteor head in the video increases slightly when the meteor flies from the image corner to the image center. In the following 19 frames (= 760 ms), down to an altitude of 116.9 km, neither a wake nor a train occurs.

Between frames 01:50:59:07 and 01:50:59:16 (for 360 ms) the meteor shows a trapezoid shape. This is quite remarkable, because this artefact – just like the "wings" of Polaris in Figure 2 – is caused alone by lens defects such as curvature of field, astigmatism and coma. The occurrence of this artefact states, firstly, that the meteor is becoming significantly overexposed at the beginning of the occurrence of the artefact and secondly, that the meteor head still appears as a point shaped object until the artefact ends. According to the camera and lens tests that were made by the authors, blooming caused by the camera sensor or the lens have to be excluded as a reason. So, after the vanishing of this artefact, from frame 01:50:59:16 on at an altitude of 94.9 km, the meteor head has to be seen as an areal object that is spatially resolved by the camera. Due the clipping caused by overexposure the exact shape of the meteor head cannot be determined from the video image, but significant hints are revealed in the following.

4.2 Wake

To differentiate the meteor head, the white wake and the green train it is evident that a colour video camera provides significant advantages. Due to the motion blur, the wake is not resolved sharply. A very short white wake can be seen at first in frame 01:50:59:05 at an altitude of 119.1 km. "White" is referred to the white balance of the camera which was daylight of approximately 6000 K. In the beginning the wake's length is shorter than the motion blur. So, its duration is less than 40 ms. In the following frames the wake becomes a little longer but is followed by the green train so quickly that they cannot be separated precisely.

Table 1 – Trajectory and additional parameters of 3414-2018.

Time code (UT) [hh:mm:ss:ff]	Distance from meteor entry at the start of frame [km]	Height [km]	Comments
01:50:58:11	−1.8	160.2	Point A
01:50:58:12	0.7	158.0	
01:50:58:13	3.1	155.8	
01:50:58:14	5.5	153.7	
01:50:58:15	8.0	151.5	
01:50:58:16	10.6	149.2	
01:50:58:17	13.2	147.0	
01:50:58:18	15.7	144.8	
01:50:58:19	18.1	142.7	
01:50:58:20	20.5	140.6	
01:50:58:21	22.9	138.4	
01:50:58:22	25.3	136.3	
01:50:58:23	27.7	134.2	
01:50:58:24	30.0	132.2	
01:50:59:00	32.5	130.0	
01:50:59:01	34.9	127.9	
01:50:59:02	37.3	125.8	
01:50:59:03	39.8	123.5	
01:50:59:04	42.3	121.4	
01:50:59:05	44.9	119.1	
01:50:59:06	47.4	116.9	
01:50:59:07	49.8	114.8	
01:50:59:08	52.3	112.6	
01:50:59:09	54.9	110.3	Point B
01:50:59:10	57.6	108.0	
01:50:59:11	60.2	105.7	
01:50:59:12	62.7	103.5	
01:50:59:13	65.1	101.4	
01:50:59:14	67.5	99.2	
01:50:59:15	70.0	97.0	
01:50:59:16	72.4	94.9	
01:50:59:17	74.8	92.8	
01:50:59:18	77.1	90.8	
01:50:59:19	79.4	88.8	
01:50:59:20	81.7	86.7	
01:50:59:21	84.0	84.8	
01:50:59:22	86.2	82.8	Point C
01:50:59:23	88.5	80.8	
01:50:59:24	90.7	78.8	Point D

Point A: indicates the point where the meteor became visible in the Geigersau video. It lies inside the integration time of this frame of 40 ms.
Point B: Meteor entry in Horní Vltavice photo
Point C: Terminal flash; distance of entry point of 87.6 km, height 81.6 km
Point D: Expiration of meteor head; distance from entry point 92.9 km, height 76.9 km

4.3 Green train

In general, a green train is caused by emission in the [O I] line at 557.7 nm. The exact maxima of the colour primaries of the Sony α7S are unknown to the authors, but it is obvious that the maximum wavelength of the green channel lies below [O I] line. Hence, the green train also affects the red channel, so the resulting colour is a slightly yellowish green.

According to Figure 1 the green train becomes visible at frame 01:50:59:07 at an altitude of 114.8 km. The green train occurs "in retrospect": the end of the green train becomes brighter in the following frames. It remains visible until frame 01:51:00:15 (= 1320 ms). The brightness of the green train has two maxima: the first around frame 01:50:59:16 and the second with the terminal flash at frame 01:50:59:22. The position of the first maximum is at the position of the meteor head in frame 01:50:59:09. The brightest parts of the first maximum of green train remain visible until frame 01:51:51:12, so this part of the green train has an overall duration of 55 frames (= 2200 ms). The position of the second maximum is at the center of the terminal flash with a strong but rapidly declining afterglow from frame 01:50:59:22 until frame 01:51:01:00 (= 1120 ms). Interestingly, the longest duration of the afterglow of the green train is not at the position of the second maximum, the terminal flash, but at the position of the meteor head at frame 01:50:59:19, three frames (= 120 ms) before the terminal flash, at an altitude of 88.8 km. Here the green train remains visible nearly as long as in

Table 2 – Trajectory parameters of 3414-2018 calculated by Juergen Michelberger, Lauffen am Neckar, Germany.

Observation site 1	Geigersau (D): Peter C. Slansky/Bernd Gaehrken		
Latitude	47.728° N		
Longitude	11.027° E		
Altitude above sea level	933 m		
Azimuth to observation site 2	55.066°		
Trajectory points	Point A	Point C	Point D
Right ascension	76.180°	197.239°	199.957°
Declination	82.608°	78.535°	77.075°
Azimuth	10.969°	355.844°	354.686°
Vertical angle	49.011°	36.679°	35.421°
Distance directly	206.9 km	133.5 km	129.6 km
Distance projected on ground	132.5 km	105.7 km	104.4 km
Observation site 2	Horní Vltavice (CZ): Juergen Michelberger/Reinhardt Wurzel		
Latitude	48.952° N		
Longitude	13.765° E		
Altitude above sea level	822 m		
Azimuth to observation site 1	237.112°		
Trajectory points	Point A	Point C	Point D
Right ascension	303.232°	291.579°	290.933
Declination	28.995°	10.308°	9.139
Azimuth	268.934°	262.715°	262.403
Vertical angle	40.918°	19.942°	18.644
Distance directly	237.1 km	226.4 km	226.9 km
Distance projected on ground	174.8 km	210.2 km	212.4 km
Base line parallax	243.7 km		
Trajectory points	Point A	Point C	Point D
Parallaxes to trajectory	66.169°	80.760°	81.313°
Trajectory points	Point A	Point C	Point D
Latitude projected to ground	48.898°	48.677°	48.663°
Longitude projected to ground	11.372°	10.922°	10.895°
Altitude above sea level	158.6 km	81.6 km	76.9 km
Trajectory points	Point A to D	Point A to C	Point C to D
Distance over ground	43.55 km	41.05 km	2.51 km
Distance along trajectory	92.9 km	87.62 km	5.28 km
Meteor duration	1.575 s	1.485 s	0.090 s
Virtual trajectory angle from observation site 1	18.091°	16.523°	1.568°
Virtual trajectory angle from observation site 2	22.967°	21.636°	1.331°
Meteor entry angle at point D	61.23°		

the first maximum. In the end the green colour blends more and more into the white of the persistent train.

The afterglow of the green train shows a relatively sharp outline with a radius of about 4 km from point C as shown in Figure 8.

4.4 Terminal flash

As was explained above, at frame 01:50:59:16 the meteor head begins to bloom. This corresponds to an altitude of 94.9 km. 6 frames later, at an altitude of 82.8 km, the meteor disintegrates in a terminal flash. During these 6 frames the brightness of the meteor increases over-exponentially.

Figure 2 shows that the terminal flash causes an overexposed and clipped meteor center in the image. The clipped area is nearly perfectly round shaped with a diameter of 188 pixels, the terminal flash does not show any motion blur. Hence, the authors assume a very sharp brightness peak of the terminal flash of less than 1/10 of a frame or less than 4 ms.

Note, that the green train extends into the overexposed center. Because a white overexposed area of an image cannot be "dimmed" by additional green light, this shows that the terminal flash is not entirely round shaped but has a dimmer part at the rear, connected to the green train. This might have the same reason as the axe-shape of the halo of the 2001 Leonid observed by Jenniskens & Stenbaek-Nielsen with 1000 fps (Jenniskens & Stenbaek-Nielsen, 2004). But due to the stronger motion blur in our case, caused by the integration time of 1/25 s, this cannot be judged precisely.

In order to investigate the nature of the clipped area the authors made a series of tests with the same camera and lens. Their volume would burst the volume of this article; the methods and the results are documented in (Slansky & Gaehrken, 2018). As a result, it was impossible to reproduce a clipped area of this size by the overexposure of a point light source alone without producing other significant artefacts like lens flares. These artefacts are missing in the images. So, only an areal light source produces a high light reproduction like the one in the video.

Figure 8 (left) shows the spatial dimensions of the terminal flash: The two yellow circles indicate a radius of 2 km (inner circle) respectively 4 km (outer circle) around point C. Each white line indicates a real distance

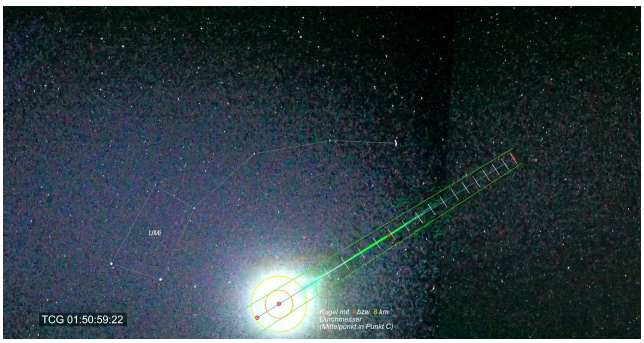

Figure 8 – Terminal flash (left). Two frames after the terminal flash (right). The two yellow circles indicate a diameter of 4 km (inner circle) and 8 km (outer circle) at point C of the trajectory. Each white line indicates a real distance along the trajectory of 5 km starting from point A (red dot on the right).

along the trajectory of 5 km starting from point A (red dot on the right). The yellow circle with the radius of 4 km fits quite well with the terminal flash. Even in the green afterglow fits to the light distribution of 3414-2018.

4.5 Afterglow of the terminal flash

The afterglow of the terminal flash is presented in Figures 9–11.

4.6 Widespread bluish sky glow

It came as a big surprise to the authors that the terminal flash was not just reflected by the sky but that a widespread bluish sky glow around the terminal flash showed a decay over up to 12 frames (= 480 ms). In the images of both cameras the bluish sky glow occurred in a very wide area around the terminal flash. To exclude camera or lens artefacts as a reason for this light effect the authors made another line of empirical tests with the same camera-lens combination. As a result, camera or lens artefacts could be excluded as a reason. The methods and results of the tests are documented in (Slansky & Gaehrken, 2018).

4.6.1 Photometry of the sky glow

To examine the brightness distribution of the meteor three separate measurements were made from each video frame: one for the meteor core in white and in green, including the meteor head, the wake, the terminal flash and its afterglow, a second one for the meteor core in green, including the green train and the green afterglow, and a third for the bluish sky glow in the red, green and blue channel. According to the huge brightness differences these measurements had to be based on different methods.

The sky glow was very dim. For its determination the opto-electronical conversion function (OECF) of the Sony α7S the original settings of the observation was measured by Peter C. Slansky with a Kodak test chart with 20 grey scales of 1/3 F-stop (Slansky, 2018b). The OECF was put into an Excel-table with the code values of the three channels RGB on the y-axis (8 Bit = 0 to 255 for red, green and blue) and the brightness in arbitrary F-stops on the x-axis. It was normalized to the sky background that was measured in the video frames before the increase of the meteor head's brightness and the terminal flash. This measurement has an error of

Figure 9 – One frame after the terminal flash. The meteor head is proceeding further from the position of the terminal flash. Note the strong green afterglow behind and around the meteor head. Its diameter is almost the same as the one of the terminal flash. Also, note the widespread bluish sky glow.

Figure 10 – Two frames after the terminal flash. The meteor head is proceeding to its terminal position where it fades away. Note the white afterglow of the wake and the strong green afterglow. Independently, the sky glow declines but remains bluish.

Figure 11 – Three frames after the terminal flash. The meteor head has faded away. Note the white afterglow of the wake and the strong green afterglow.

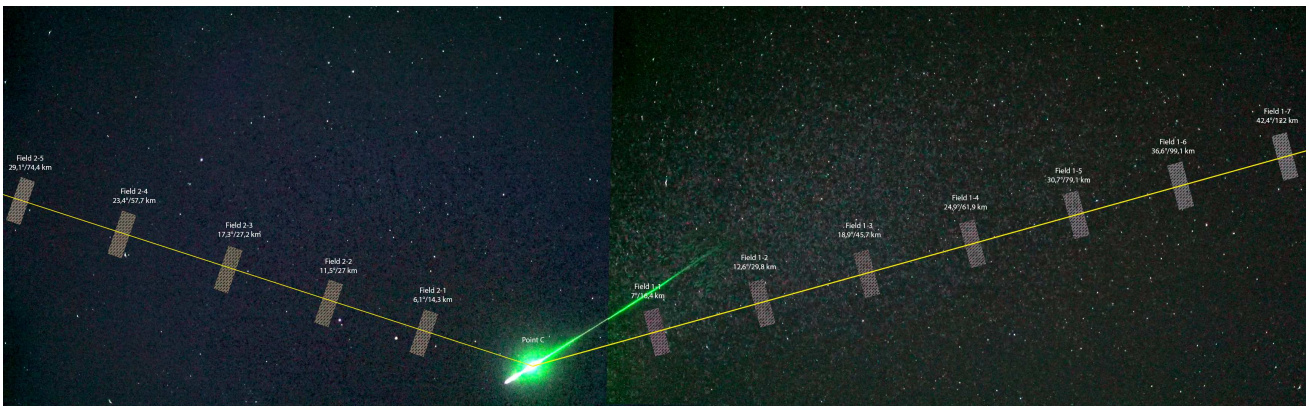

Figure 12 – Arrangement of the measurement fields for the sky glow for both cameras. In order to reduce the influence of the apparent image noise each field is 40 × 160 pixels wide, with the code values averaged. The distance from point C is indicated as an angle as well as a distance along the respective yellow line rectangular to the line from the camera to point C. A positive sign indicates the direction with the trajectory (to the left), a negative sign against the trajectory (to the right).

less than 1/10 of an F-stop or less than 7% at code values higher than 4.

The measurement of the sky glow was done separately for both cameras in an alignment of measurement fields of 40 × 160 pixels. Inside these fields the code values were averaged to eliminate the influence of the image noise. The distances of the centers of the fields from point C are indicated as an angle as well as a distance along the respective yellow line rectangular to the line from the camera to point C. A positive sign indicates the direction with the trajectory (to the left), a negative sign against the trajectory (to the right).

Left from point C five measurement fields were aligned (Table 3).

Table 3 – Measurement fields from camera 2.

Field	Angle from point C	Distance from point C	Camera
2-1	5.6°	13 km	2
2-2	12°	29 km	2
2-3	18°	43 km	2
2-4	23°	57 km	2
2-5	30°	76 km	2

Right from point C seven measurement fields were aligned. Because field 1 of camera 1 suffered strongly from sensor amplifier glowing it was superseded by field 2- -1 of camera 2 (Table 4).

Table 4 – Measurement fields from cameras 1 and 2.

Field	Angle from point C	Distance from point C	Camera
2- −1	−7.0°	−16 km	2
1-2	−13°	−30 km	1
1-3	−19°	−46 km	1
1-4	−25°	−62 km	1
1-5	−31°	−79 km	1
1-6	−37°	−99 km	1
1-7	−42°	−122.1 km	1

4.6.2 Photometry of the meteor core

Due to the strong overexposure with huge numbers of clipped pixels the brightness of the meteor core – the green train, the wake, the terminal flash and the green afterglow – had to be measured by another method. Their brightness should be compared to the bluish sky glow only relatively. Because the numbers of clipped pixels are proportional to the overexposed areas this numbers were taken as an indicator. For a comparative diagram this number was also calculated to F-stops. An absolute calibration was not necessary because the comparison was made relatively. Because of the significant differences in the distribution between the white light – the wake, the terminal flash and their afterglow – and the green light – the green train and its afterglow – separate counting of clipped pixels was made for white and green. For the white overexposed area all pixels with RGB code values 255/255/255 were counted and for the green overexposed area all pixels with RGB code values X/255/X were counted with X ≠ 255 ("green only"). The exactness of measurement of this method has not been calculated.

In this article all photometric measurements rely on images recorded by cameras. So, their results are expressed in F-stops, not in magnitudes, because magnitudes go back to the nonlinearity of the human eye: One magnitude represents a physical brightness increase (or decrease) by a factor 2.5, to be taken as a perceptual brightness increase (or decrease) by the human eye by a factor 2. Both expressions can be converted to each other easily: One F-stop equals 3/4 magnitude, one magnitude equals 4/3 F-stops.

4.6.3 Temporal brightness distribution of the sky glow

As can be seen from Figures 19 and 20, the temporal progress of brightness of the sky glow is related to the brightness progress of the meteor core but not in a linear way. Neither does the brightness of sky glow follow the brightness of the white terminal flash and the white afterglow nor the brightness of the green train and green afterglow. Also, the sky glow keeps its bluish colour nearly constantly.

In Figure 19 (bottom curves) the high value of the red channel of field 2-5 has to be ignored because it goes back to sensor amplifier glowing of the camera.

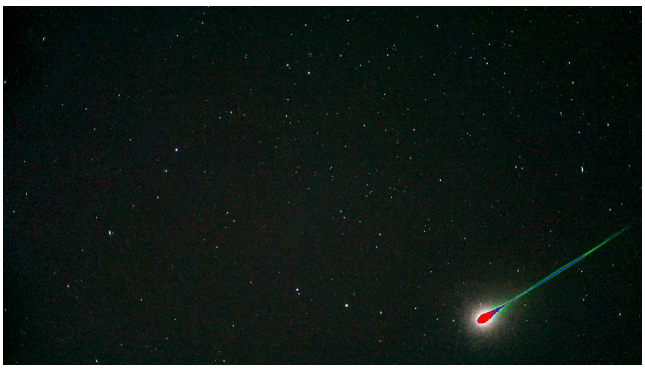

Figure 13 – Video frame 01:50:59:20 of camera 2, two frames before the terminal flash. The white overexposed pixels are indicated in red, the green overexposed pixels (green only) in blue. Counting reveals 1144 overexposed pixels white = 8.2 arbitrary F-stops and 1067 overexposed pixels green (only) = 8.1 arbitrary F-stops. The white amount and the green only amount are almost equal.

Figure 14 – Frame 01:50:59:21 of camera 2, one frame before the terminal flash: 3554 overexposed pixels white = 9.8 arbitrary F-stops and 2636 overexposed pixels green = 9.4 arbitrary F-stops. The white amount begins to dominate the green one.

Figure 15 – Frame 01:50:59:22 of camera 2, terminal flash: 11076 overexposed pixels white = 11.4 arbitrary F stops and 6077 overexposed pixels green = 10.6 arbitrary F-stops. The terminal flash is much stronger in white than in green. This cannot be caused by a strong green overexposure, because than a green halo would be seen. But the halo around the terminal flash is white. Additionally, a bluish sky glow appears. (Also, the averaging of the code values inside the measurement fields can be seen.) The rectangular structures around and behind the meteor head are data compression artefacts caused by the camera.

Figure 16 – Video frame 01:50:59:23 of camera 2, one frame after the terminal flash: 3172 overexposed pixels white = 9.6 arbitrary F-stops and 5255 overexposed pixels green = 10.4 arbitrary F-stops. It is quite remarkable that even in the first frame after the terminal flash the green begins to dominate the white due to its much longer persistence.

Figure 17 – Video frame 01:50:59:24 of camera 2, two frames after the terminal flash: 978 overexposed pixels white = 7.9 arbitrary F-stops and 5433 overexposed pixels green = 10.4 arbitrary F-stops. Only two frames after the terminal flash the dominance of the green over the white has become drastic.

Figure 18 – Video frame 01:51:00:00 of camera 2, three frames after the terminal flash: 495 overexposed pixels white = 7.0 arbitrary F-stops and 4770 overexposed pixels green = 10.2 arbitrary F-stops. As can be seen from this sequence, the white light and the green light have different temporal distributions: The white has a higher maximum but a more sudden decline compared to the green with a lower maximum but a longer persistence. The widespread sky glow does not follow the change in colour of the meteor core from white to green only.

Figure 20 shows the brightness of the sky glow in the direction against the trajectory.

Please note that in Figure 20 field 2- -1 of camera 2 was used instead of field 1 of camera 1, because the former suffered strongly from sensor amplifier glowing.

As can be seen from Figures 15–18 and graphs in Figures 19 and 20, until the terminal flash the brightness of the white parts of the meteor core (black circles in Figure 19) dominate the green parts (dark green triangles in Figure 19). In the first frame after the ter-

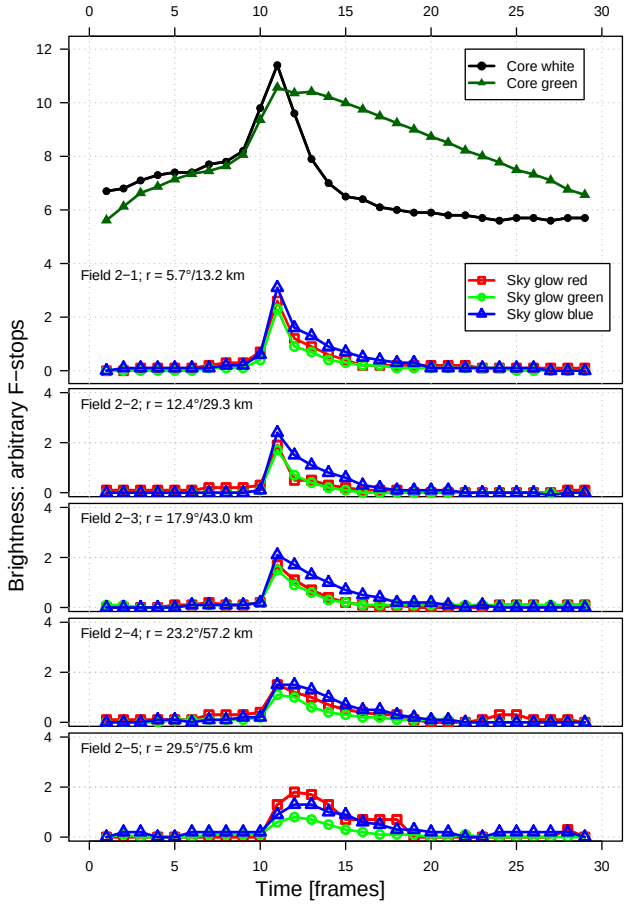

Figure 19 – The brightness of the sky glow in the direction with the trajectory.

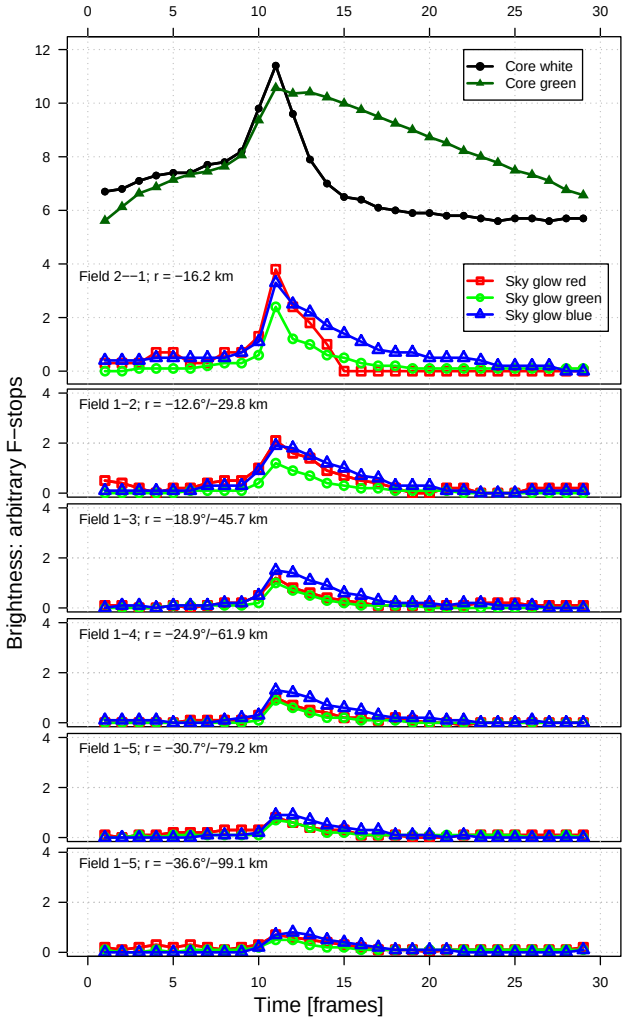

Figure 20 – The brightness of the sky glow in the direction against the trajectory.

minal flash the green parts begin to dominate, showing a much longer persistence than the white parts of the core. But the sky glow does not follow this drastic transient. It keeps its bluish colour throughout. Also, its persistence lasts longer than that of the white parts of the core (see black curve in Figure 19).

To the knowledge of the authors, such a phenomenon has not been reported before.

Because of this temporal brightness and colour development, the sky glow cannot be caused be reflection of the meteor in the earth's atmosphere alone. Diffuse reflection can only do a small contribution to this sky glow. Mainly, it must have other physical reasons.

Another remarkable detection is the spatial dimensions of the sky glow. As expressed in Figures 19 and 20, it is visible with a similar temporal development in both cameras and in all 12 measurement fields. The most remote field of camera 1 is field 1-7 with an angular distance from point C of 42.4° or 122 km, of camera 2 it is field 2-5 with an angular distance from point C of 29.5° or 75.6 km.

A last striking issue is a dark void inside the widespread sky glow with its center about 8.5° or 20 km of from point C on the upper left side. According to Figure 19 (fields 2-2, 2-3, and 2-4), beginning in the frame after the terminal flash – frame 12 in the respective tables – until frame 17 the sky glow is remarkably darker in fields 2-1 and 2-2 than in the more remote fields 2-3 and 2-4. This dark void remains stationary for about five frames = 200 ms. It cannot be explained by camera or lens artefacts.

4.7 Persistent train

The persistent train of 3414-2018 started at a height of 100 km and ended at a height of 79 km with a length of 30 km. He was recorded with two cameras, the Sony α7s in video mode 25 fps and a Canon EOS M that provided a photo series. The EOS M is an APS-C format camera. It was equipped with a 2.8/50mm lens. The exposure time was 15 seconds at ISO 3200.

On the Sony video, the persistent train is completely visible and its development is easy to follow (Slansky, 2018c). The end of the wake and the beginning of the persistent train are difficult to separate. The brightness measurement of the persistent train starts two seconds after the end of the terminal flash. At this time, only small parts of the track burned out and the remains of the wakes have disappeared.

The EOS M exposure time of 15 s was 375 times longer than the exposure time of the Sony α7s of 1/25 s. On the other side, the sensitivity of the EOS M of ISO 3200 and that of the Sony ISO 409 000 and the lens of the EOS M had an aperture of 2.8 while the lens of the Sony had an aperture of 1.4. But the longer

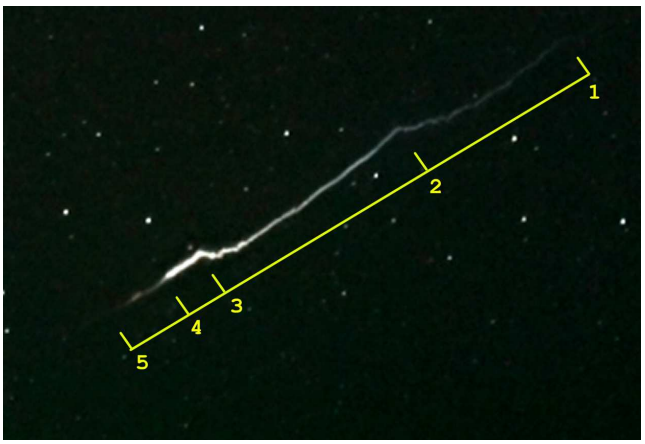

Figure 21 – The persistent train in an overlay of 25 video frames at time code 01:51:06.

Table 5 – Height of points 1–5 in Figure 21.

Point in Figure 21	1	2	3	4	5
Height [km]	100	92	82	81	79

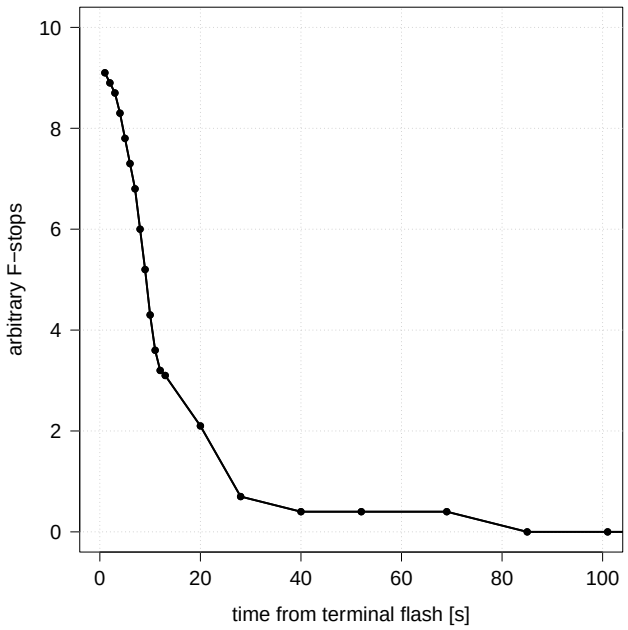

Figure 22 – Brightness development of the persistent train measured over 2.5 minutes.

exposure time of the EOS M and the lower ISO setting provided a better signal-to-noise-ratio and higher colour saturation. So, in the photo series of the EOS M shown in Figure 3 the persistent train could be detected better, over a duration time of 7 minutes before the photo series was stopped. The colour gradient from blue to red that is typical for a fresh persistent train is still clearly visible on the first picture after the fall. On the second picture after the fall, the blue has faded and all other pictures show a uniform brown-yellowish colour.

In Figure 21 five points are marked. Table 5 shows their respective height.

At 01:51:06 UT, six seconds after the terminal flash, the persistent train is showing signs of disintegration, as it breaks up into several sections. The reason for the kinks at points 2 and 3 in Figure 22 are different vertical winds in the high atmosphere.

The first and the last section of the train faded very fast. At points 2, 3 and 4 an attempt to measure the development of the brightness was made. However, it lacked a three-dimensional model that enabled a calculation of the changing column density with the perspective of the photo series. Therefore, at least the brightness development of the total curve was determined. This measurement was corrected with the OECF of the video camera (see Section 4.6.1). The result is shown in Figure 22. It shows three sectors: In the first 12 seconds there is a strong decrease in brightness by a factor 63 = 6 F-stops. After that, the curve flattens considerably: Between the twelfth and the twenty-eighth second the brightness drop is only factor 5.6 = 2.5 F-stops. From the twenty-eighth second on the brightness drop is very flat. The persistent train is still visible but cannot be measured properly for the next 100 seconds.

4.8 Radio Observation

Wolfgang Kinzel sent the authors a radio diagram of a long meteor trail echo. By the exact time and the long trail echo there could be no mistake: That was 3414-2018. He had observed the fireball from Dessau, Saxony-Anhalt, 51°48'06.46" N / 12°15'22.01" E, 65 m altitude, with a four-element yagi antenna in the 2-meter band at 143.050 MHz, pointed to the GRAVES radar in France, with an azimuth of 221° SW, elevation 20°, 3 m over ground level. The distance Dessau-GRAVES is 694 km. Because the main direction of the GRAVES radar is south, the trail echo must come from one of the northern secondary lobes of the radar.

The interpretation of the radiogram was given by Wolfgang Kaufmann, Algermissen. Figure 23 shows two typical meteor head echoes, A and C. B is a meteor trail echo of about 100 ms. This duration meets the majority of radio meteors. According to the exact timing, D is the trail echo of 3414-2018. It lasts 43 s and has a Doppler shift of 35 Hz at the maximum. The Doppler shift is estimated to be caused mainly by wind drift that affects different parts of the trail in different heights in different ways and directions. This is estimated to a tree-dimensional warping of the trail that can be seen in the photo series of the persistent train (Figure 3), too. Additionally, the radio waves reflected by the different trail segments reach the receiver with different phasing. This explains the oscillation of the signal amplitude. At the end the trail echo occurs more and more interrupted. This might also go back to wind drift changing the geometry of radio wave reflection. The radiogram does not show indications for fragmentation.

Parallel observations of meteorites in the visual and the radio range are still rare and a comparison with the visual ZHRs is difficult. But with only one video observation and one radio observation from different positions three-dimensional calculations cannot be made. In order to better understand the context, especially in the interpretation of the Doppler shift, it would make sense to expand parallel observations, as well in video as in radio.

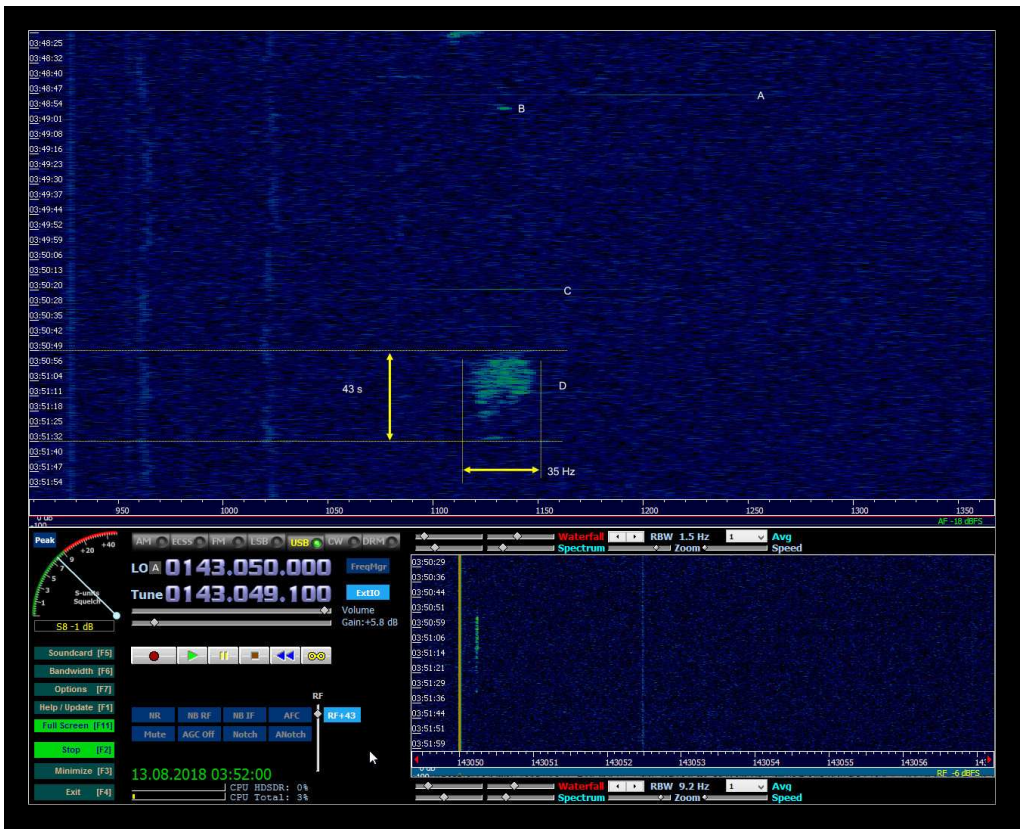

Figure 23 – Radiogram of 3414-2018 by Wolfgang Kinzel, Dessau, Saxony-Anhalt, 51°48'06.46" N / 12°15'22.01" E, 65 m altitude. The observation was made with a four-element yagi antenna in the 2-meter band at 143.050 MHz, pointed to the GRAVES radar in France, with an azimuth of 221° SW and elevation 20°, 3 m over ground level.

5 Discussion

The light distribution of 3414-2018 shows several remarkable peculiarities. The observations were possible only by the use of two very high sensitive cameras in video mode with full HD resolution in colour.

Referring to Figure 2 the terminal flash shows a nearly perfect circular shape, but with a significant green strangling on the rear which is connected directly to the green train. This might have similar reasons as the axe-shape of the halo of the 2001 Leonid, observed by Jenniskens & Stenbaek-Nielsen (2004). Due to the stronger motion blur caused by an integration time of 1/25 s this cannot be judged precisely (Jenniskens & Stenbaek-Nielsen, 2004).

The spatial dimensions of the terminal flash and the green afterglow of 3414-2018 with a radius up to 4 km are exceptional. This goes back to advances in the observing technique compared to observations with older analog monochrome CCD cameras with SD resolution that are still widely in use in meteor observation.

For the 2001 Leonid observed by Jenniskens & Stenbaek-Nielsen, Šiljić et al. (2018) report a brightness gradient of 1 km from the meteor heads center the brightness fallen down to 1/30 of the maximum at an altitude of 104.8 km. (The measurement was not executed to wider distances.) It has to be taken into account that the exposure of the images has a huge influence on measurements like this. It would be very valuable to detect brightness gradients of meteors via high dynamic range imaging.

There is also reasonable conformity between fireballs 3414-2018 and EN120812 observed by Spurný et al. (2014): Both show terminal flashes with a very sharp brightness increase on nearly the same altitude (Table 6).

According to Wurzel & Michelberger (2005) the air density is increasing significantly at this altitude.

Spurný et al. (2014) divided the appearance of high altitude meteors into three distinct phases: diffuse, intermediate and sharp. The diffuse phase was observed and described by Gaehrken/Michelberger for a high altitude Leonid 2002 (Gaehrken & Michelberger, 2003). According to this, the similarities between 3414-2018 and EN120812 indicate similar physical formation conditions.

The diffuse, widespread bluish sky glow of 3414-2014 has been recorded by two cameras independently: Camera 2 with the terminal flash in its field of view as well as camera 1 with the terminal flash outside its field of view. The bluish sky glow can be seen up to an angle of 42° – respectively a distance of 122 km – from the point of the terminal flash. Its bluish colour does not follow the drastic change in colour from the white terminal flash to the green afterglow with a much longer persistence. Hence, diffuse reflection contributes only a minor part to the sky glow, but cannot be its major physical reason. Also, the temporal development of the brightness as well as the colour of the sky glow does neither follow the development of the white part of the meteor core nor the one of the green part. Again, the

Table 6 – Brightness developments along the trajectories of Perseid fireballs 3414-2018 and EN120812.

	Altitude of entry	Altitude of terminal flash	Altitude of expiration
3414-2018	158.6 km	81.6 km	76.9 km
EN120812	170.2 km	82.7 km	78.6 km

physical reasons must be different from diffuse reflection in the earths' atmosphere alone.

There are different scientific approaches for the explanation of the physical nature of meteors' light emissions, for example electric charge and magnetic fields around the meteor (Šiljić et al., 2018), UV-radiation (Jenniskens, 2004) or X-rays (Smirnov, 2015). Because the authors are amateur meteor observers they will not exceed their competence by speculation. But they are ready to discuss and share their observations and data with every interested scientist.

Acknowledgements

The authors want to thank Juergen Michelberger and Reinhardt Wurzel for their engaged cooperation on the observation and analysis of 3414-2018, especially for the calculation of the trajectory. The authors also thank Wolfgang Kinzel for obtaining his radio observation and Wolfgang Kaufmann for its interpretation. Thank also goes to Rudolf Sanda, Austria, Christ Steyaert, Belgium, and Giancarlo Tomezzoli, Germany, for additional information about the radiogram.

References

Gaehrken B. (2018). "Perseiden 2018". http://www.astrode.de/8perseiden18a.htm

Gaehrken B. and Michelberger J. (2003). "A bright, high altitude 2002 Leonid". *WGN, Journal of the IMO*, **31:5**, 137–138.

Hughes D. W. (1995). "The Perseid meteor shower". *Earth Moon and Planets*, **68**, 31–70.

IMO (2014). "Events in 2014: 3638-2014". https://fireballs.imo.net/members/imo_view/event/2014/3638

IMO (2017). "Events in 2017: 4299-2017". https://fireballs.imo.net/members/imo_view/event/2017/4299

IMO (2018). "Events in 2018: 3414-2018". https://fireballs.imo.net/members/imo_view/event/2018/3414

Jenniskens P. (2004). "Meteor storms as a window on the delivery of extraterrestrial organic matter to the early Earth". In Norris R. P. and Stoothman F. H., editors, *Bioastronomy 2002: Life Among Stars, IAU Symposium*, volume 213. IAU, pages 281–288.

Jenniskens P. and Stenbaek-Nielsen H. C. (2004). "Meteor wake in high frame-rate images and implications for the chemistry of ablated organic compounds". *Astrobiology*, **4:1**, 95–108.

Rendtel J. (2017). "2018 Meteor Shower Calendar". IMO_INFO(2-17).

Slansky P. C. (2016). "Meteor film recording with digital film cameras with large CMOS sensors". *WGN, Journal of the IMO*, **44:6**, 190–197.

Slansky P. C. (2018a). "The efficiency of cameras for video meteor observation and a theoretical contribution and a practical comparison between the Watec 120N+ and the Sony α7S". *WGN, Journal of the IMO*, **46:1**, 24–29.

Slansky P. C. (2018b). "Opto-electronical conversion function of the Sony α7S with standard gamma". http://slansky.userweb.mwn.de/bereiche/astronomie/aufnahmetechniken/bilder/oecf_sony-a7s.pdf .

Slansky P. C. (2018c). "Time lapse sequence of 3414-2018". http://slansky.userweb.mwn.de/bereiche/astronomie/meteore/perseiden-bolid_13-08-2018_03-51_03a.html

Slansky P. C. (2019). "SCAMPI - Single Camera Measurement of the Population Index". In ??, editor, *Proceedings of the International Meteor Conference, Pezinok, Slovakia, 2018.* International Meteor Organization, page ??

Slansky P. C. and Gaehrken B. (2018). "Camera test of the Sony α7S with a Canon FD 1.4/50 mm lens about blooming of overexposed highlights in regard of the video observation of fireball 3414-2018". http://slansky.userweb.mwn.de/bereiche/astronomie/aufnahmetechniken/bilder/camera-test_sony-a7s_3414_2018.pdf

Smirnov V. A. (2015). "About the nature of meteor flares". *Odessa Astronomical Publications*, **28**, 58.

Spurný P., Shrbený L., Borovička J., Koten P., Vojáček V., and Štork R. (2014). "Bright Perseid fireball with exceptional beginning height of 170 km observed by different techniques". *Astronomy & Astrophysics*, **563**, A64.

Šiljić A., Lunić F., Teklić J., and Vinković D. (2018). "Proton-induced halo formation in charged meteors". *MNRAS*, **481**, 2858–2870.

Wurzel R. (2019). "Eine Feuerkugel der Extraklasse". *Sterne und Weltraum*, **58:8**, 62–69.

Wurzel R. and Michelberger J. (2005). "Earthgrazer – Wunder des Himmels". *Sterne und Weltraum*, **44:11**, 76–83.

Handling Editors: Željko Andreić and Javor Kac

Preliminary results

Results of the IMO Video Meteor Network — May 2018

Sirko Molau[1], Stefano Crivello, Rui Goncalves, Carlos Saraiva, Enrico Stomeo, Jörg Strunk, Javor Kac

During 2018 May, cameras of the IMO Video Meteor Network recorded almost 15 000 meteors in nearly 7 500 hours of observing time. Activity of the η-Aquariids was well covered by the Network cameras. The flux density profile is presented for the full activity period between April 20 and May 28. It matches well to the average profile obtained during years 2014–2017. The shower presents a maximum plateau with over 30 meteoroids per 1000 km^2 per hour between May 5 and 9. New options of the online MeteorFlux tool are also presented.

Received 2019 May 25

1 Introduction

There is no other month during which the climatic conditions are as stable as in May. We can, at least, see that the observational results showed only little variation over the past four years. The effective observing time fluctuated between 7 000 and 7 800 hours, during which we recorded between 16 500 and 18 300 meteors. The 7 500 observing hours, amassed by 40 observers with 78 video cameras in May 2018, match perfectly to the average. It was only the yield that was a little lower with 15 000 meteors (Table 1 and Figure 1). A quick look at the monthly summary presented in Figure 1 shows us that the first half of May was slightly better than the second. 80% of the cameras managed to observe during twenty or more observing nights, which is a top-class result. All observers apart from those from Slovenia enjoyed great observing conditions.

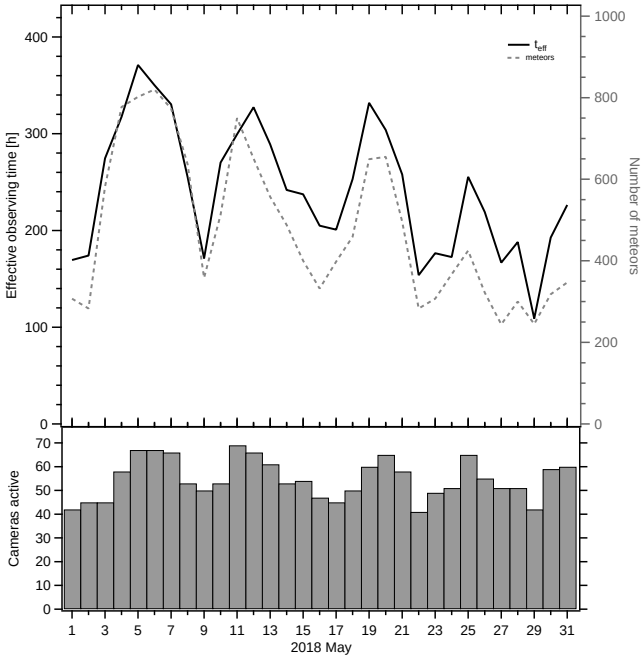

Figure 1 – Monthly summary for the effective observing time (solid black line), number of meteors (dashed gray line) and number of cameras active (bars) in 2018 May.

2 η-Aquariids

The η-Aquariids are the highlight of May, and we have reported about this shower several times (Molau et al., 2012; Molau et al., 2013; Molau et al., 2014; Molau et al., 2015; Molau et al., 2016; Molau et al., 2017). Whereas we see little from this shower in Central Europe, it is the shower of the year in the southern hemisphere. Figure 2 shows the activity profile of the η-Aquariids in 2018 covering the whole activity period. Around April 27 the activity starts to rise, and by the transition from between April to May it has already risen to 10 meteoroids per 1 000 km^2 per hour. Between May 5 and 9 we see a distinct plateau of high activity with over 30 meteoroids per 1 000 km^2 per hour. Thereafter the activity is quickly declining and reaches the base level near May 18. There are significant fluctuations in early May, which can be attributed to an insufficient dataset between May 1 and 3, though.

The population index of the η-Aquariids can only be determined over longer time intervals, because even during the maximum nights our cameras record too few meteors. Near the peak it has a value of about $r = 2.2$, whereas at the same time the sporadic meteors show a population index of $r = 2.6$ (Figure 3). In 2017 we had obtained similar r-values of 2.0 and 2.6, respectively (Molau et al., 2017).

Because of their radiant position, the η-Aquariids are of particular interest. Those few shower members which can be observed from Central Europe, always occur at low radiant altitudes. Effects such as the zenith exponent, which have a strong impact on the flux density at low radiant altitudes, can be analysed particularly well with this shower. Figure 4 shows three peak nights in detail. We do not see any systematic variation, which implies that the zenith exponent of 1.5 is of the right order.

On the other hand, most observations are hampered by twilight, which leaves some uncertainty if that has an impact on the analysis. We could exclude that with an additional selection criterion in MeteorFlux. We could define a minimum stellar limiting magnitude, for example, to filter out observation at dawn. In addition, we could configure a maximum radiant altitude beside

[1]Abenstalstr. 13b, 84072 Seysdorf, Germany.
Email: sirko@molau.de

IMO bibcode WGN-473-molau-vidmay
NASA-ADS bibcode 2019JIMO...47...93M

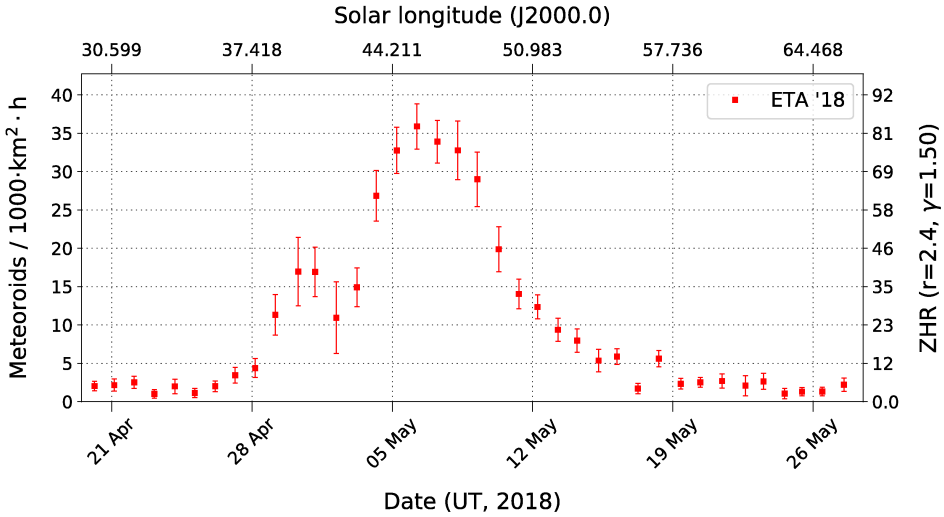

Figure 2 – Flux density profile of the η-Aquariids in May 2018, derived from video data of the IMO Network.

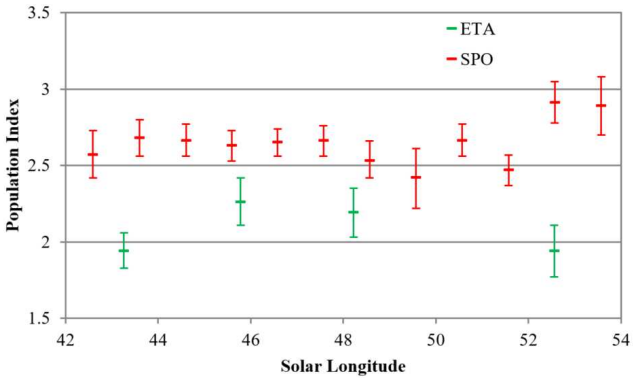

Figure 3 – Population index profile of the η-Aquariids and sporadic meteors in May 2018.

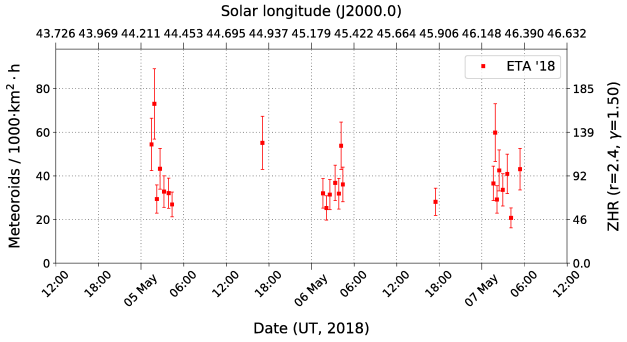

Figure 4 – High resolution flux density profile of the η-Aquariids on 2018 May 4–7.

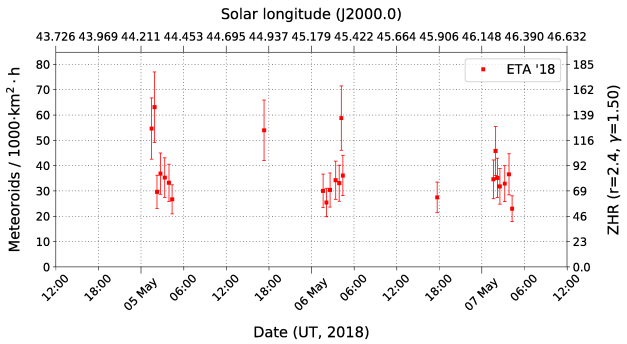

Figure 5 – High resolution flux density profile of the η-Aquariids on 2018 May 4–7, using only intervals with a stellar limiting magnitude better than 2.0 magnitude.

the already existing minimum altitude, to analyse other showers like the Quadrantids, Perseids or Geminids under similar radiant altitudes.

Unfortunately, both of the programmers that developed MeteorFlux and migrated it on to a new AWS instance, withdrew from the project a long time ago. Many change requests have been put on hold since 2013, and lacking knowledge of JavaScript, Python and PostgreSQL, Sirko never dared to approach the code.

During the ETA analysis of 2018, however, Sirko decided to have a look at the source code, anyway, and to implement these new filters by copy&paste from existing code fragments. The result was quite encouraging and after two evenings the rough structure of the code had been understood and additional filters had been successfully implemented. Figure 5 shows the same flux density profile as before, but only including observing intervals with a stellar limiting magnitude of mag 2 or better. The flux density profile changes only a little, and hence twilight does not seem to have a significant impact on the activity profile.

Spurred on this success, Sirko dared to immediately implement the next selection criterion, the option to select individual cameras, which had been needed for many years. This functionality was implemented in one evening, with the option to select the camera set by the observer, country and continent being added later.

Euphorically, Sirko then addressed a third aspect. Often, the requirement is not to create a single activity graph, but to compare two flux density profiles with one another. The aforementioned fluctuations of the η-Aquariids in early May 2018 are a nice example. We want to compare the profiles with the average of the previous years to see if this is a recurring structure. Previously, both graphs would be generated independently of each other, and then merged together using Photoshop. Now, the two profiles can be generated via MeteorFlux in a single graph. Not only can the observing year be varied, but also the other parameters used to generate the reference profile. This allows for a range of new analysis options, which we want to use intensively in the future, e.g.:

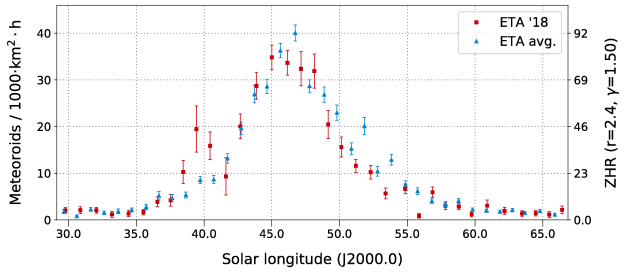

Figure 6 – Flux density profile of the η-Aquariids in 2018 (red) and in the average of 2014–2017 (blue), derived from video data of the IMO Network.

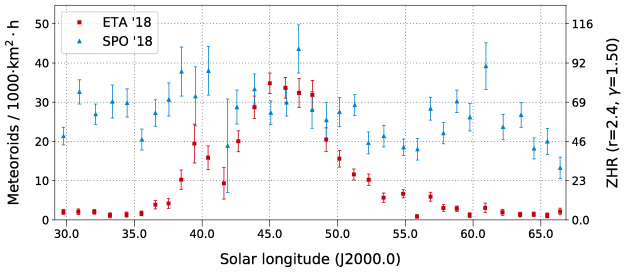

Figure 7 – Flux density profile of the η-Aquariids (red) and sporadic meteors (blue) in May 2018.

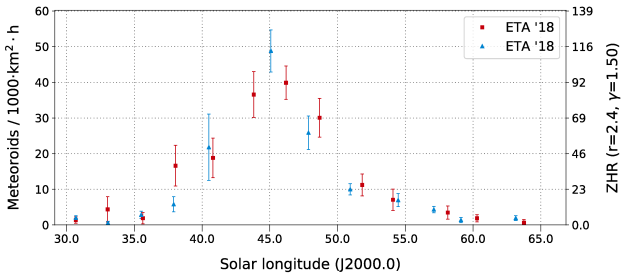

Figure 8 – Flux density profile of the η-Aquariids in May 2018, recorded by video cameras in Germany (red) and Italy (blue).

- To compare the profile of a meteor shower from one year with the average for other years (and adapt the binning of the reference profile to lower or higher temporal resolution depending on the meteor number).
- The mean activity profile of years with new moon and full moon can be compared to search for systematic deviations.
- To compare the activity of two meteor showers over the same time interval, e.g. for a meteor shower and sporadic meteors, or for the Northern and Southern Taurids. For better visibility, the reference shower can be offset and scaled linearly.
- Selecting different binning parameters to compare a low resolution and high-resolution activity profile.
- Observers can compare the results of their camera(s) with those of other cameras. The results of cameras from different countries can also be compared.
- Data with good and poor limiting magnitudes can be compared, as can observations with low and high radiant altitudes.
- The impact of different zenith exponents can be studied directly in a single graph.

These functional extensions were implemented in three evenings. The following Figures 6–8 give a few examples for the new functions, which can now be used by everyone at `meteorflux.org`.

So far, all functions have been implemented primarily by copy&paste, but now Sirko feels sufficiently optimistic to also attempt step by step extensions which require some new code.

References

Molau S., Crivello S., Goncalves R., Saraiva C., Stomeo E., and Kac J. (2016). "Results of the IMO Video Meteor Network - May 2016". *WGN, Journal of the IMO*, **44:5**, 174–178.

Molau S., Crivello S., Goncalves R., Saraiva C., Stomeo E., and Kac J. (2017). "Results of the IMO Video Meteor Network - May 2017, and flux density calculation". *WGN, Journal of the IMO*, **45:6**, 144–148.

Molau S., Kac J., Berko E., Crivello S., Stomeo E., Igaz A., and Barentsen G. (2012). "Results of the IMO Video Meteor Network - May 2012". *WGN, Journal of the IMO*, **40:4**, 144–148.

Molau S., Kac J., Berko E., Crivello S., Stomeo E., Igaz A., Barentsen G., and Goncalves R. (2013). "Results of the IMO Video Meteor Network - May 2013". *WGN, Journal of the IMO*, **41:4**, 133–138.

Molau S., Kac J., Crivello S., Stomeo E., Barentsen G., Goncalves R., and Igaz A. (2014). "Results of the IMO Video Meteor Network - May 2014". *WGN, Journal of the IMO*, **42:4**, 150–154.

Molau S., Kac J., Crivello S., Stomeo E., Barentsen G., Goncalves R., Saraiva C., Maciejewski M., and Maslov M. (2015). "Results of the IMO Video Meteor Network - May 2015". *WGN, Journal of the IMO*, **43:5**, 152–155.

Handling Editor: Javor Kac

Code	Name	Location	Camera	FOV [°²]	Stellar LM [mag]	Eff.CA [km²]	Nights	Time [h]	Meteors
ARLRA	Arlt	Ludwigsfelde/DE	Ludwig2 (0.8/8)	1475	6.2	3779	28	124.5	440
BERER	Berkó	Ludányhalászi/HU	Hulud1 (0.8/3.8)	5542	4.8	3847	5	34.9	90
BIATO	Bianchi	Mt. San Lorenzo/IT	Omsl1 (1.2/4)	6435	4.0	1705	23	118.1	149
BOMMA	Bombardini	Faenza/IT	Mario (1.2/4.0)	5794	3.3	739	28	117.0	287
BREMA	Breukers	Hengelo/NL	Mbb3 (0.75/6)	2399	4.2	699	24	121.8	145
BRIBE	Klemt	Herne/DE	Hermine (0.8/6)	2374	4.2	678	25	103.7	175
		Bergisch Gladbach/DE	Klemoi (0.8/6)	2286	4.6	1080	25	104.9	174
CARMA	Carli	Monte Baldo/IT	Bmh2 (1.5/4.5)*	4243	3.0	371	20	80.9	225
CASFL	Castellani	Monte Baldo/IT	Bmh1 (0.8/6)	2350	5.0	1611	21	82.0	107
CINFR	Cineglosso	Faenza/IT	Jenni (1.2/4)	5886	3.9	1222	22	62.6	273
CRIST	Crivello	Valbrevenna/IT	Arci (0.8/3.8)	5566	4.6	2575	23	83.0	157
			Bilbo (0.8/3.8)	5458	4.2	1772	24	86.0	173
			C3P8 (0.8/3.8)	5455	4.2	1586	21	72.6	126
			Stg38 (0.8/3.8)	5614	4.4	2007	26	110.8	337
ELTMA	Eltri	Venezia/IT	Met38 (0.8/3.8)	5631	4.3	2151	13	51.2	103
FORKE	Förster	Carlsfeld/DE	Akm3 (0.75/6)	2375	5.1	2154	19	92.7	229
GONRU	Goncalves	Foz do Arelho/PT	Farelho1 (0.75/4.5)	2286	3.0	208	10	53.0	30
		Tomar/PT	Templar1 (0.8/6)	2179	5.3	1842	28	153.0	395
			Templar2 (0.8/6)	2080	5.0	1508	25	140.9	301
			Templar3 (0.8/8)	1438	4.3	571	25	148.6	128
			Templar4 (0.8/3.8)	4475	3.0	442	24	130.3	267
			Templar5 (0.75/6)	2312	5.0	2259	24	134.8	262
GOVMI	Govedič	Središče ob Dravi/SI	Orion2 (0.8/8)	1447	5.5	1841	24	76.4	106
			Orion3 (0.95/5)	2665	4.9	2069	4	1.1	6
			Orion4 (0.95/5)	2662	4.3	1043	22	49.1	62
HERCA	Hergenrother	Tucson/US	Salsa3 (0.8/3.8)	2336	4.1	544	28	241.4	358
HINWO	Hinz	Schwarzenberg/DE	Hinwo1 (0.75/6)	2291	5.1	1819	26	111.3	220
IGAAN	Igaz	Budapest/HU	Hupol (1.2/4)	3790	3.3	475	18	84.5	38
JONKA	Jonas	Budapest/HU	Husor (0.95/4)	2286	3.9	445	27	121.2	80
			Husor2 (0.95/3.5)	2465	3.9	715	22	97.5	87
KACJA	Kac	Kamnik/SI	Cvetka (0.8/3.8)*	4914	4.3	1842	13	47.4	103
			Rezika (0.8/6)	2270	4.4	840	16	52.9	167
			Stefka (0.8/3.8)	5471	2.8	379	13	45.8	68
		Kostanjevec/SI	Metka (0.8/12)*	715	6.4	640	21	91.5	120
LOJTO	Łojek	Grabniak/PL	Pav57 (1.0/5)	1631	3.5	269	14	76.2	219
MACMA	Maciejewski	Chełm/PL	Pav35 (0.8/3.8)	5495	4.0	1584	26	91.0	143
			Pav36 (0.8/3.8)*	5668	4.0	1573	28	140.7	252
			Pav43 (0.75/4.5)*	3132	3.1	319	20	61.0	58
			Pav60 (0.75/4.5)	2250	3.1	281	27	139.5	286

Table 1 – Observers contributing to 2018 May data of the IMO Video Meteor Network. Eff.CA designates the effective collection area; the overall number of nights is the number of nights with at least one camera operating, the overall observing time and number of meteors are sums over all cameras.

Table 1 – Observers contributing to 2018 May data of the IMO Video Meteor Network – continued from previous page.

Code	Name	Location	Camera	FOV [°²]	Stellar LM [mag]	Eff.CA [km²]	Nights	Time [h]	Meteors
MARRU	Marques	Lisbon/PT	Cab1 (0.75/6)	2362	4.8	1517	28	149.4	339
			Ran1 (1.4/4.5)	4405	4.0	1241	21	86.3	163
MOLSI	Molau	Seysdorf/DE	Avis2 (1.4/50)*	1230	6.9	6152	27	108.3	603
			Escimo2 (0.85/25)	155	8.1	3415	26	120.6	198
			Mincam1 (0.8/8)	1477	4.9	1084	22	91.5	319
		Ketzür/DE	Remo1 (0.8/8)	1467	6.5	5491	22	102.5	376
			Remo2 (0.8/8)	1478	6.4	4778	23	111.3	433
			Remo3 (0.8/8)	1420	5.6	1967	23	125.7	381
			Remo4 (0.8/8)	1478	6.5	5358	23	123.0	559
MORJO	Morvai	Fülöpszállás/HU	Huful (1.4/5)	2522	3.5	532	23	107.6	90
MOSFA	Moschini	Rovereto/IT	Rover (1.4/4.5)	3896	4.2	1292	12	42.8	35
NAGHE	Nagy	Budapest/HU	Hukon (0.8/3.8)	5500	4.0	1575	24	54.9	157
		Piszkéstető/HU	Hupis (0.8/3.8)	5615	4.0	1524	29	91.7	233
OCHPA	Ochner	Albiano/IT	Albiano (1.2/4.5)	2944	3.5	358	11	35.8	46
OTTMI	Otte	Pearl City/US	Orie1 (1.4/5.7)	3837	3.8	460	20	103.6	89
PERZS	Perkó	Becsehely/HU	Hubec (0.8/3.8)*	5498	2.9	460	21	108.5	125
ROTEC	Rothenberg	Berlin/DE	Armefa (0.8/6)	2366	4.5	911	25	121.7	203
SARAN	Saraiva	Carnaxide/PT	Ro1 (0.75/6)	2362	3.7	381	25	140.9	134
			Ro2 (0.75/6)	2381	3.8	459	21	117.4	173
			Ro3 (0.8/12)	710	5.2	619	23	131.8	246
			Ro4 (1.0/8)	1582	4.2	549	16	77.8	57
			Sofia (0.8/12)	738	5.3	907	23	102.3	147
SCALE	Scarpa	Alberoni/IT	Leo (1.2/4.5)*	4152	4.5	2052	22	75.2	61
SCHHA	Schremmer	Niederkrüchten/DE	Doraemon (0.8/3.8)	4900	3.0	409	26	103.3	176
SLAST	Slavec	Ljubljana/SI	Kayak1 (1.8/28)	563	6.2	1294	18	53.2	123
			Kayak2 (0.8/12)	741	5.5	920	12	47.6	24
STOEN	Stomeo	Scorze/IT	Min38 (0.8/3.8)	5566	4.8	3270	26	71.8	276
			Noa38 (0.8/3.8)	5609	4.2	1911	24	85.5	249
			Sco38 (0.8/3.8)	5598	4.8	3306	26	86.3	322
STRJO	Strunk	Herford/DE	Mincam2 (0.8/6)	2354	5.4	2751	25	118.7	321
			Mincam3 (0.8/6)	2338	5.5	3590	25	120.6	174
			Mincam4 (0.8/6)	2306	5.0	1412	24	115.5	129
			Mincam5 (0.8/6)	2349	5.0	1896	25	123.9	212
			Mincam6 (0.8/6)	2395	5.1	2178	24	111.8	217
TEPIS	Tepliczky	Agostyán/HU	Huago (0.75/4.5)	2427	4.4	1036	24	105.6	145
			Humob (0.8/6)	2388	4.8	1607	26	98.4	157
WEGWA	Wegrzyk	Nieznaszyn/PL	Pav78 (0.8/6)	2286	4.0	778	20	68.1	91
YRJIL	Yrjölä	Kuusankoski/FI	Finexcam (0.8/6)	2337	5.5	3574	10	21.2	47
ZAKJU	Zakrajšek	Petkovec/SI	Tacka (0.8/12)	714	5.3	783	21	93.0	70
* active field of view smaller than video frame						Overall	31	7 490.0	14 846

Results of the IMO Video Meteor Network — June 2018

Sirko Molau[1], *Stefano Crivello, Rui Goncalves, Carlos Saraiva, Enrico Stomeo, Jörg Strunk, Javor Kac*

During 2018 June, cameras of the IMO Video Meteor Network recorded over 14 000 meteors during more than 5 700 hours of observing time. The current database contains about 260 single station Daytime Arietids, corresponding to flux density of about 15 meteoroids per 1 000 km^2 per hour, which in turn corresponds to a ZHR in the upper two-digit range.

Received 2019 June 18

1 Introduction

June 2018 delivered a below average yield for the IMO Network video observers, although this is not obvious from a glimpse at the results (Table 1 and Figure 1). We see a continuation of the trend which started earlier this year: The typically dominating Portuguese observers had to make do with twenty and sometimes clearly fewer observing nights, whereas observers in Germany and Poland collected well above twenty nights. Only our Italian team enjoyed their usual perfectly clear skies. Overall 47 of 76 video cameras recorded meteors during twenty or more observing nights. The effective observing time of 5 700 hours fell 15% to 25% short of that of the previous four years, and the 14 000 meteors represented a decrease of even 25% to 35%. Indeed, it is the worst June result since 2011 when the IMO Network still consisted of fewer than fifty cameras.

[1]Abenstalstr. 13b, 84072 Seysdorf, Germany.
Email: sirko@molau.de

IMO bibcode WGN-473-molau-vidjun
NASA-ADS bibcode 2019JIMO...47...98M

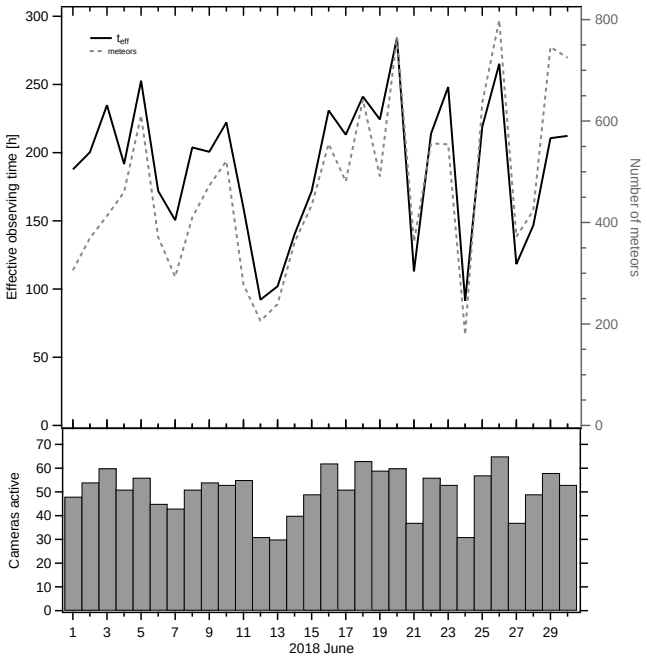

Figure 1 – Monthly summary for the effective observing time (solid black line), number of meteors (dashed gray line) and number of cameras active (bars) in 2018 June.

2 Daytime Arietids

In addition, with respect to meteor showers, June has only little to offer. There are the Daytime Arietids, which have been targeted by visual and video observers for several years (Rendtel, 2014), in order to normalize the hourly rates obtained from radar data with the ZHR and flux density in the optical domain. Due to the exceptionally short observing window, the data is still rudimentary even after 8 years. If we include all observing intervals starting at 0° radiant altitude, all IMO Network cameras have in total accumulated just 17 500 km^2 h of effective collection area during 2 250 hours of effective observing time. That is about as much effective collection area as two powerful video cameras collect during a single Geminid night. Given this, the reported number of 260 shower meteors is quite substantial. It yields a flux density of about 15 meteoroids per 1 000 km^2 per hour, corresponding to a ZHR in the upper two-digit range. Due to the exceptional circumstances the error bars are quite large, though. In particular we would need to find out how big the sporadic pollution is in this case.

3 June Bootids

The yield of the June Bootids, the second meteor shower of June, is also negligible, but for a different reason. This shower presents significant outbursts only once in a few years (last time 2004), and otherwise it is below the detection threshold. Both in 2018 and in the long-term average of 2011–2017, the flux density was below 0.1 meteoroids per 1 000 km^2 per hour (Figure 2), which should reflect the sporadic background. In fact, if we plot the long-term average June Bootid and sporadic profiles (the latter one scaled down by a factor of 500), the profiles match almost perfectly (Figure 3).

But which observers have contributed which data set to this graph? The online FluxViewer now not only provides a data table, but also provides additional statistics on the contributing cameras and observers. Hence, we know that Stg38 of Stefano Crivello provided most effective collection area for Figure 2. The cameras of Rui Goncalves, Enrico Stomeo and Maurizio Eltri were equally successful data collectors for the June Bootids.

Unfortunately, the backlog of IMO Network observing reports has significantly increased recently – the deficit is now almost one year. In order to make interested researchers not wait too long, we have introduced a second database in FluxViewer. Alongside the regular database, which contains complete and double-

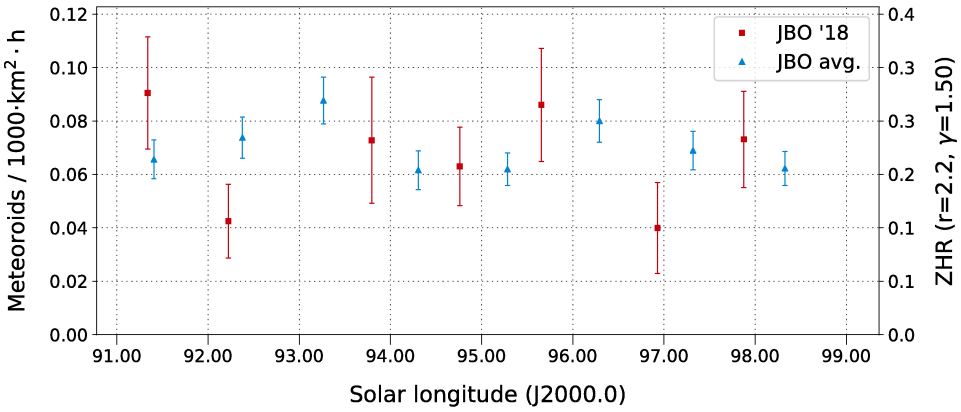

Figure 2 – Flux density profile of the June Bootids in 2018 (red) and the average for 2011–2017 (blue), derived from video data of the IMO Network.

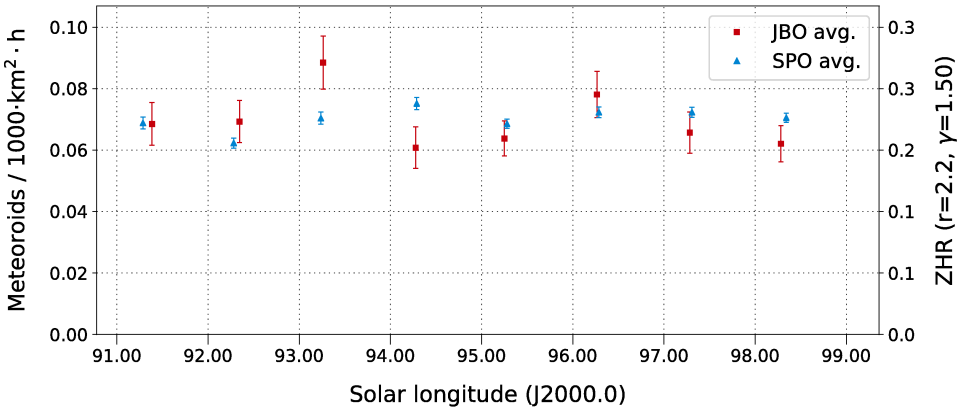

Figure 3 – Comparison of the activity profile of the June Bootids and sporadic meteors (downscaled by a factor of 500) with the average for the years 2011–2018.

checked data up to the corresponding monthly report (currently: June 2018) the observers can upload their video data into the temporary database on their own. These data are more up-to-date (sometimes to the day), but incomplete and not double-checked. Via a check-box in the `meteorflux.org` web interface researchers can decide which of the two data sets they would like to use.

References

Rendtel J. (2014). "Daytime meteor showers". In Rault J.-L. and Roggemans P., editors, *Proceedings of the International Meteor Conference, Giron, France, 18-21 September 2014*. pages 93–97.

Handling Editor: Javor Kac

Code	Name	Location	Camera	FOV [°²]	Stellar LM [mag]	Eff.CA [km²]	Nights	Time [h]	Meteors
ARLRA	Arlt	Ludwigsfelde/DE	Ludwig2 (0.8/8)	1475	6.2	3779	23	66.6	279
BIATO	Bianchi	Mt. San Lorenzo/IT	Omsl1 (1.2/4)	6435	4.0	1705	23	119.7	211
BOMMA	Bombardini	Faenza/IT	Mario (1.2/4.0)	5794	3.3	739	28	146.0	479
BREMA	Breukers	Hengelo/NL	Mbb3 (0.75/6)	2399	4.2	699	17	58.2	100
BRIBE	Klemt	Herne/DE	Hermine (0.8/6)	2374	4.2	678	20	62.7	158
		Bergisch Gladbach/DE	Klemoi (0.8/6)	2286	4.6	1080	18	69.7	149
CARMA	Carli	Monte Baldo/IT	Bmh2 (1.5/4.5)*	4243	3.0	371	24	109.3	439
CASFL	Castellani	Monte Baldo/IT	Bmh1 (0.8/6)	2350	5.0	1611	22	109.4	230
CINFR	Cineglosso	Faenza/IT	Jenni (1.2/4)	5886	3.9	1222	28	159.0	630
CRIST	Crivello	Valbrevenna/IT	Arci (0.8/3.8)	5566	4.6	2575	27	108.3	270
			Bilbo (0.8/3.8)	5458	4.2	1772	28	114.3	289
			C3P8 (0.8/3.8)	5455	4.2	1586	25	87.7	231
			Stg38 (0.8/3.8)	5614	4.4	2007	26	101.2	431
ELTMA	Eltri	Venezia/IT	Met38 (0.8/3.8)	5631	4.3	2151	25	87.7	199
FORKE	Förster	Carlsfeld/DE	Akm3 (0.75/6)	2375	5.1	2154	15	28.6	137
GONRU	Goncalves	Foz do Arelho/PT	Farelho1 (0.75/4.5)	2286	3.0	208	3	9.6	5
		Tomar/PT	Templar1 (0.8/6)	2179	5.3	1842	20	92.4	244
			Templar2 (0.8/6)	2080	5.0	1508	20	89.2	185
			Templar3 (0.8/8)	1438	4.3	571	16	66.7	51
			Templar4 (0.8/3.8)	4475	3.0	442	19	84.6	180
			Templar5 (0.75/6)	2312	5.0	2259	20	70.3	142
GOVMI	Govedič	Središče ob Dravi/SI	Orion2 (0.8/8)	1447	5.5	1841	19	60.9	107
			Orion3 (0.95/5)	2665	4.9	2069	6	6.8	10
			Orion4 (0.95/5)	2662	4.3	1043	18	35.0	48
HERCA	Hergenrother	Tucson/US	Salsa3 (0.8/3.8)	2336	4.1	544	23	181.7	357
HINWO	Hinz	Schwarzenberg/DE	Hinwo1 (0.75/6)	2291	5.1	1819	20	77.8	142
IGAAN	Igaz	Budapest/HU	Hupol (1.2/4)	3790	3.3	475	10	35.8	23
JONKA	Jonas	Budapest/HU	Husor (0.95/4)	2286	3.9	445	17	51.6	56
			Husor2 (0.95/3.5)	2465	3.9	715	20	60.3	69
KACJA	Kac	Kamnik/SI	Cvetka (0.8/3.8)*	4914	4.3	1842	13	54.7	139
			Rezika (0.8/6)	2270	4.4	840	13	57.3	198
			Stefka (0.8/3.8)	5471	2.8	379	13	55.7	110
		Kostanjevec/SI	Metka (0.8/12)*	715	6.4	640	16	66.9	95
LOJTO	Łojek	Grabniak/PL	Pav57 (1.0/5)	1631	3.5	269	3	9.0	20
MACMA	Maciejewski	Chełm/PL	Pav35 (0.8/3.8)	5495	4.0	1584	22	64.0	135
			Pav36 (0.8/3.8)*	5668	4.0	1573	22	81.0	195
			Pav43 (0.75/4.5)*	3132	3.1	319	22	40.6	61
			Pav60 (0.75/4.5)	2250	3.1	281	22	82.6	232

Table 1 – Observers contributing to 2018 June data of the IMO Video Meteor Network. Eff.CA designates the effective collection area; the overall number of nights is the number of nights with at least one camera operating, the overall observing time and number of meteors are sums over all cameras.

Table 1 – Observers contributing to 2018 June data of the IMO Video Meteor Network – continued from previous page.

Code	Name	Location	Camera	FOV [°²]	Stellar LM [mag]	Eff.CA [km²]	Nights	Time [h]	Meteors
MARRU	Marques	Lisbon/PT	CAB1 (0.75/6)	2362	4.8	1517	26	141.6	319
			RAN1 (1.4/4.5)	4405	4.0	1241	14	56.2	90
MOLSI	Molau	Seysdorf/DE	AVIS2 (1.4/50)*	1230	6.9	6152	23	85.3	647
			ESCIMO2 (0.85/25)	155	8.1	3415	24	105.5	223
			MINCAM1 (0.8/8)	1477	4.9	1084	9	31.8	78
		Ketzür/DE	REMO1 (0.8/8)	1467	6.5	5491	26	77.5	359
			REMO2 (0.8/8)	1478	6.4	4778	24	77.1	353
			REMO3 (0.8/8)	1420	5.6	1967	25	89.0	322
			REMO4 (0.8/8)	1478	6.5	5358	24	87.1	445
MORJO	Morvai	Fülöpszállás/HU	HUFUL (1.4/5)	2522	3.5	532	20	91.6	74
MOSFA	Moschini	Rovereto/IT	ROVER (1.4/4.5)	3896	4.2	1292	22	95.7	118
NAGHE	Nagy	Budapest/HU	HUKON (0.8/3.8)	5500	4.0	1575	21	56.8	112
		Piszkéstető/HU	HUPIS (0.8/3.8)	5615	4.0	1524	22	32.4	119
OCHPA	Ochner	Albiano/IT	ALBIANO (1.2/4.5)	2944	3.5	358	21	83.5	119
OTTMI	Otte	Pearl City/US	ORIE1 (1.4/5.7)	3837	3.8	460	18	48.6	167
PERZS	Perkó	Becsehely/HU	HUBEC (0.8/3.8)*	5498	2.9	460	18	71.9	83
ROTEC	Rothenberg	Berlin/DE	ARMEFA (0.8/6)	2366	4.5	911	22	72.9	103
SARAN	Saraiva	Carnaxide/PT	RO1 (0.75/6)	2362	3.7	381	17	70.2	91
			RO2 (0.75/6)	2381	3.8	459	15	67.4	106
			RO3 (0.8/12)	710	5.2	619	17	88.0	172
			RO4 (1.0/8)	1582	4.2	549	15	53.6	47
			SOFIA (0.8/12)	738	5.3	907	19	41.2	79
SCALE	Scarpa	Alberoni/IT	LEO (1.2/4.5)*	4152	4.5	2052	25	91.6	89
SCHHA	Schremmer	Niederkrüchten/DE	DORAEMON (0.8/3.8)	4900	3.0	409	22	77.9	190
SLAST	Slavec	Ljubljana/SI	KAYAK1 (1.8/28)	563	6.2	1294	20	78.2	200
			KAYAK2 (0.8/12)	741	5.5	920	21	95.3	85
STOEN	Stomeo	Scorze/IT	MIN38 (0.8/3.8)	5566	4.8	3270	25	78.5	373
			NOA38 (0.8/3.8)	5609	4.2	1911	25	100.6	317
			SCO38 (0.8/3.8)	5598	4.8	3306	29	82.9	366
STRJO	Strunk	Herford/DE	MINCAM2 (0.8/6)	2354	5.4	2751	22	73.0	240
			MINCAM3 (0.8/6)	2338	5.5	3590	19	61.1	124
			MINCAM4 (0.8/6)	2306	5.0	1412	19	64.8	96
			MINCAM5 (0.8/6)	2349	5.0	1896	20	71.0	144
			MINCAM6 (0.8/6)	2395	5.1	2178	20	64.1	126
TEPIS	Tepliczky	Agostyán/HU	HUAGO (0.75/4.5)	2427	4.4	1036	21	80.4	129
			HUMOB (0.8/6)	2388	4.8	1607	19	77.6	122
WEGWA	Wegrzyk	Nieznaszyn/PL	PAV78 (0.8/6)	2286	4.0	778	15	30.8	45
ZAKJU	Zakrajšek	Petkovec/SI	TACKA (0.8/12)	714	5.3	783	21	98.5	124
* active field of view smaller than video frame						Overall	30	5 714.1	14 032

History

A History of Meteor Reports in The Astronomer magazine: part 4: 2000–2012

Tracie Heywood[1]

The magazine "*The Astronomer*" (TA) is a monthly magazine published in the UK whose aim is the rapid publication of observations made by amateur astronomers. It was first published in 1964. This is the fourth article in a series that provide an overview of the magazine's meteor content and covers the years 2000–2012.

Received 2019 May 26

1 Introduction

The 1990s had concluded with a meteor storm from the Leonids that had peaked within a few minutes of the time predicted in advance by Asher & McNaught. This seemed to herald a new era – one in which meteor observers might know in advance when meteor storms and other significant meteor outbursts were likely to occur. Observers would thus be able to travel to the relevant parts of the world in order to see these outbursts at their best.

2 Leonids

Most significantly, Asher and McNaught had predicted that, although there would be no meteor storm in November 2000, additional Leonid meteor storms would occur in 2001 and 2002. These would be occurring more than three years after the parent comet had passed through perihelion. Some of these storms would be occurring more than 24 hours after passing through the "traditional" Leonid peak.

2001: Two main storm peaks are predicted to occur during 2001 November 18 by Asher & McNaught. The first is predicted for $09^{h}55^{m}$ UT and will favour observers in North America. The second is predicted for $18^{h}13^{m}$ UT and will favour observers in eastern Asia and the western Pacific. Both storm peaks are observed, although the first actually peaks close to $10^{h}30^{m}$ UT and the second peaks at around $18^{h}20^{m}$ UT. The discrepancies are slightly larger than those for the 1999 peak, but are nevertheless sufficiently small so as not to have left travelling observers feeling misled.

Many reports of the storm appear in the 2001 December (The Astronomer, 2001) and 2002 January (The Astronomer, 2002a) issues. Paul Jones (Florida) and Mike Reynolds (California) report their observations of the first storm, while Ron Schirato, Andrew Pearce (both Australia), Hazel McGee (Palau) and Michael Gill (Japan) report on the second storm. The front cover of the December issue (Mobberley, 2001) shows a Leonid fireball imaged by Martin Mobberley from Palau as it passed through Orion. Martin's detailed account of the Explorers expedition to Palau appears in the February issue (Mobberley, 2002).

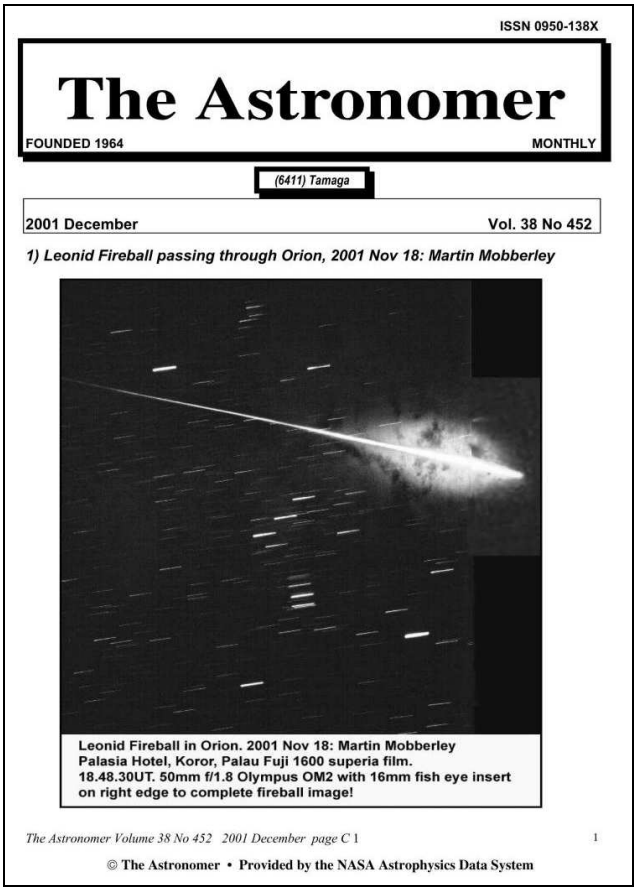
ISSN 0950-138X

The Astronomer

FOUNDED 1964 MONTHLY

(6411) Tamaga

2001 December Vol. 38 No 452

1) Leonid Fireball passing through Orion, 2001 Nov 18: Martin Mobberley

Leonid Fireball in Orion. 2001 Nov 18: Martin Mobberley
Palasia Hotel, Koror, Palau Fuji 1600 superia film.
18.48.30UT. 50mm f/1.8 Olympus OM2 with 16mm fish eye insert
on right edge to complete fireball image!

The Astronomer Volume 38 No 452 2001 December page C 1 1

Figure 1 – December 2001 issue cover.

2002: The Earth is once again set to encounter both filaments that produced Leonid storms in 2001, but observing conditions will be less favourable with a 15-day old Moon brightening the sky background. Both encounters will occur during 2002 November 19, with the predicted time of $03^{h}53^{m}$ UT for the first peak favouring observers in western Europe and western Africa and the second peak, predicted for $10^{h}29^{m}$ UT, favouring observers in the western parts of North America. Subsequent analyses find the storms having peaked close to $04^{h}10^{m}$ UT and $10^{h}50^{m}$ UT. The indications are that the peak ZHRs, though clearly reaching storm level, were lower than in 2001 and those observers who had also seen the 2001 peak report that the bright moonlight made the 2002 storm appear less spectacular. Nevertheless, a good number of reports appear in the 2002 December issue (The Astronomer, 2002b), in-

[1]20 Hillside Drive, Leek, ST13 8JQ, UK.
Email: tracieheywood832@gmail.com

IMO bibcode WGN-473-heywood-ta4
NASA-ADS bibcode 2019JIMO...47..102H

cluding those from Bjorn Granslo (Norway), Alexander Baransky (Ukraine), Andrew Elliott (UK) and Hazel McGee (UK). For once, several parts of the UK have had clear skies!

2006: Although no further storms are predicted after 2002, an enhancement in Leonid rates, comparable with typical Perseid peak levels, is predicted for shortly before 05^h UT on 2006 November 19. The 2006 December issue (The Astronomer, 2006) reveals that from the UK, Neil Bone sees the enhancement, while Alastair McBeath and Tony Markham are clouded out an hour or so before the peak. Bill Ward and Tom McEwan escape the UK cloud by travelling to Spain and see the peak from Calar Alto.

3 Giacobinids

No Draconid meteor storm had been seen in 1998 when the parent comet 21P/Giacobini-Zinner had last passed through perihelion, but significant Draconid activity is considered likely for the 2005 and 2011 returns. In the event, the 2005 November issue (The Astronomer, 2005) reports that the outburst at around 17^h UT was somewhat limited and came too early for UK based observers, with Alastair McBeath only reporting a small number of Draconids later that evening. The 2011 outburst is more significant and, peaking near 20^h UT, is more conveniently timed for observers in the UK. Unfortunately, as the 2011 November issue reports (The Astronomer, 2011b), there was extensive cloud cover across the UK that evening. A few observers were lucky, however, and enjoyed fortuitously timed cloud breaks.

4 Routine Meteor Watches

In a continuation of the trend seen during the 1980s and 1990s, visual meteor observing sees a further decline. Meteor Watches are now largely confined to the days surrounding the maxima of the major meteor showers and some issues contain no meteor reports. Perseids reports are extensive in many September issues, but most other showers fare less well with the weather. The 2007 January issue (The Astronomer, 2007) reveals that Alastair McBeath and Tom Lloyd-Evans had made use of clear skies to observe the Ursid outburst during the evening of 2006 December 22. There is also quite good coverage of the Leonids in the 2004 December issue (The Astronomer, 2004) and of the Lyrids in the 2012 May issue (The Astronomer, 2012c).

5 Articles

The number of meteor related articles during this period is quite small. Martin Mobberley's account of the 2001 Leonids in the 2002 February issue (TA5) is followed by a gap of over a decade before Tony Markham's overview of "The Challenge of Observing Meteors and Fireballs Visually" appears in the 2012 June (Markham, 2012b) and 2012 July issues (Markham, 2012c). Tony Markham also provides summaries of IMC 2010 in Armagh in the 2010 October issue (Markham, 2010a) and IMC 2012 in La Palma in the 2012 October issue (Markham, 2012a).

6 New meteor showers?

Reports of possible new meteor radiants have appeared in TA from time to time over the decades. These have nearly always been based on visual observations by a single observer and virtually none of these radiants have been reported again in later years. The advent of new technology, accurately capturing large numbers of meteor images now starts to make a difference. Many new meteor shower radiants, based on video and radar observations, are listed in IAU Circulars. This gives the impression that there could be a bonanza of new meteor showers for visual observers to follow – but which of these are real and occur annually ... and how active are these new showers?

In the 2008 February issue (The Astronomer, 2008), Tony Markham cautions readers regarding a list of 13 new meteor showers that had recently been added to the IAU meteor shower list and points out that these will almost certainly only show very low naked-eye ZHRs. Further caution is again made in the 2009 June issue (The Astronomer, 2009a) following the addition of another 11 meteor showers.

The 2009 July (The Astronomer, 2009b) issue refers to a BBC news report which suggested that a meteor shower lasting for around 30 minutes was seen from southern England during the evening of 2009 June 15. It notes that subsequent investigations by the BAA Meteor Section have revealed that the most likely explanation was that a single fireball had occurred. It is likely that the 30-minute spread in times was simply due to the scatter that is often seen in reports from visual witnesses.

7 Non-meteors

Distant aircraft contrails illuminated from below can be a source of spurious ("long duration") fireball reports, particularly during the late autumn and early winter months when the morning twilight coincides with many people being outdoors. A particularly notable aircraft related example is mentioned in the 2003 November issue (The Astronomer, 2003). This involves an event which even fooled the NASA staff who publish the "Astronomy Picture of the Day", who later needed to backtrack on their original description (Nemiroff & Bonnell, 2003). Neil Bone and Alastair McBeath both cast doubt on NASA's meteor related explanation and support the idea postulated elsewhere that this was related to the Concorde aircraft heading out west over the coast, Alastair commenting the it was most likely related to its "near-supersonic climb with afterburners on".

Iridium Flares and Sky Lanterns continue to generate spurious Fireball reports. In the 2009 August (The Astronomer, 2009c) and 2010 August issues (The Astronomer, 2010) readers are reminded as to how to differentiate between these and genuine fireballs.

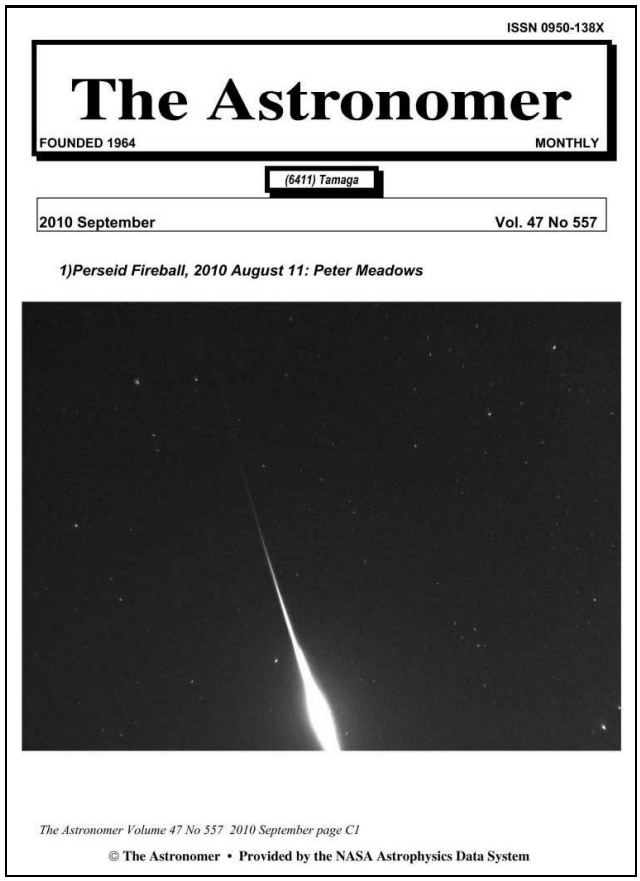

Figure 2 – September 2010 issue cover.

8 Fireballs

Overall, the number of fireball reports shows a decline on previous decades. However, a few still do appear. In the 2001 December issue (McBeath, 2001), Alastair McBeath provides a summary of the reports of the 2001 October 27–28 fireball, while the reports of the 2010 December 8 fireball in the 2011 January issue (The Astronomer, 2011a) and the 2012 March 3 fireball in the 2012 March issue (The Astronomer, 2012a) also include Alastair's summaries of observations collected by the Society for Popular Astronomy's Meteor Section and his analyses to determine the ground tracks. Mention is made in the latter case of the magnitude discrepancies between the reports collected by Alastair (mostly mag −4 to mag −10) and those reported by the American Society's fireball report form (mostly "brighter than the Full Moon").

The most widely seen fireball during this period is the 2012 September 21st fireball. Alastair McBeath's preliminary analysis of this event appears in the 2012 October issue (The Astronomer, 2012b). This long-duration event is found to have started over the North Sea, crossed northern England and Ireland and ended over the Atlantic Ocean.

9 Images

Several bright meteors and fireballs appear on the covers of TA during this period. Notable examples include Martin Mobberley's image in the 2001 December issue of a Leonid fireball (Mobberley, 2002), Figure 1, Peter Meadows' image in the September 2010 issue of a Perseid fireball (Meadows, 2010), Figure 2, Bill Ward's image in the 2010 November issue of an Orionid fireball (Ward, 2010) and Peter Meadows' image in the 2011 December issue of a Leonid fireball (Meadows, 2011).

10 Odds & Ends

Miscellaneous other meteor-related items also appear. These include Tony Markham's overview in the 2010 February issue of the effect of ageing on Limiting Magnitude estimates (Markham, 2010b), Alastair McBeath's comments in the 2010 May issue regarding the decline in UK-based meteor observing (McBeath, 2010) and Guy Hurst's notes in the 2012 October issue regarding the history of a large meteorite held by Salisbury Museum (Hurst, 2012).

11 New technology

Although CCD imaging had become the norm in most areas of amateur astronomy during the 1990s, technical limitations significantly delayed it's take-up by meteor observers, with film-based imaging persisting well into the first decade of the 21st century, especially, it seems, in the UK. The situation isn't helped by the untimely deaths of Steve Evans (March 2008) and Andrew Elliott (November 2010), two observers who had been leading UK pioneers of video imaging during the 1980s and 1990s.

In the 2006 June issue (Fischer & McBeath, 2006), Daniel Fischer highlights the excellent progress that has been made elsewhere using tools such as MetRec, while emphasizing the need for coordinated visual and video observations in order to help resolve issues with the determination of ZHRs from video records. In the same issue, Alastair McBeath notes that these analysis aids now mean that the main deterrent for potential video observers is less one of time involved in the analysis and is now more related to the cost of the equipment and of its operation. He also notes that video methods are starting to replace visual plotting as the method for radiant structure analyses.

Some progress is being made in the UK. Bill Ward mentions in his Leonid report in the 2006 December issue (Ward, 2006) that he has been experimenting for a couple of years with Watec cameras and motion detection software to pick up fireballs. He reports that his video system picked up 24 Leonids and 5 sporadics during the enhanced maximum in the early hours of 2006 November 19th.

The covers of the 2007 September issue illustrate the persistence of film use. They feature two meteor images and although with one (Ward, 2007) has been captured digitally by Bill Ward using a Watec 120 camera, the other (Bone, 2007) has been imaged by Neil Bone using Kodak Gold 400 ISO film.

Signs of the progress that is soon to come appear in the 2011 December issue (Meadows et al., 2011). Peter Meadows reports the results that he obtained during the Leonids using an automated Imaging Source monochrome DMK AU03 camera. These include a se-

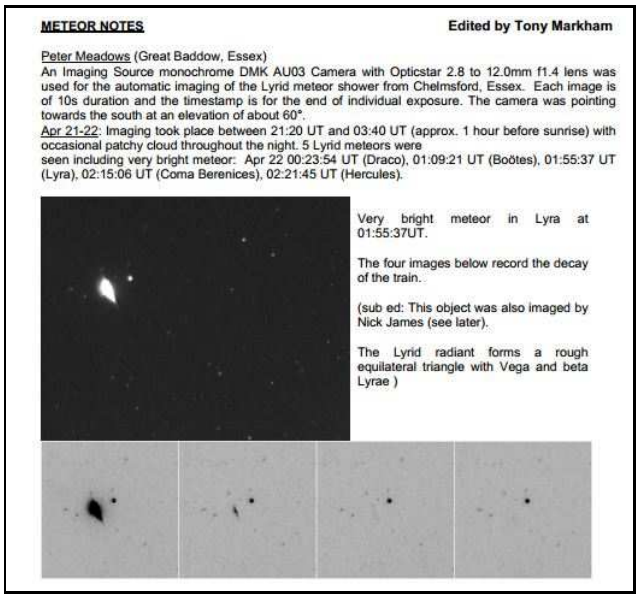

Figure 3 – Peter Meadows' image of a bright Lyrid and four images of its decaying train.

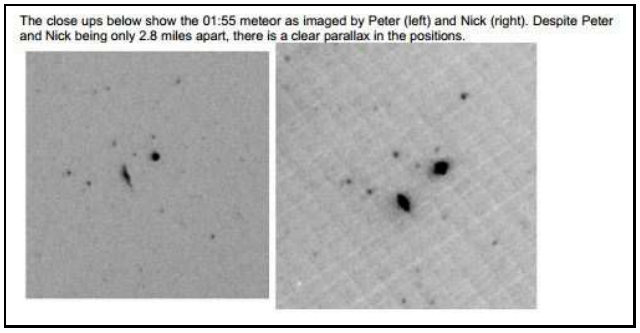

Figure 4 – Image comparison of the fireball captured by Peter Meadows and by Nick James, revealing its parallax against the star background.

quence of 20 images showing the decay of the train from a Leonid fireball. In the same issue, Nick James presents images that are created from stacks of individual video frames and Bill Ward reports that, after two years of trying, he has finally captured a spectrum that is bright enough for him to extract a spectrum intensity plot and to identify the source of the most prominent emission lines. Meteor images are now starting to play an increasing part of the Meteor Notes content. Images by Peter and Nick of the 2012 Lyrids appear in the May 2012 issue (The Astronomer, 2012c), Figures 3 & 4 and many images of bright Perseids captured by Peter, Nick and Bill appear in the 2012 September issue (Meadows et al., 2012).

12 In Conclusion

Leaving aside the meteor storms of 2001 and 2002 and a number of smaller meteor outbursts, meteor observing in the UK seems very much "in the doldrums" during most of the period covered by this article. In the 2010 May issue (Hurst, 2012), Alastair McBeath notes *"too few observers have made routine visual meteor watches to allow UK-only analyses of anything other than the occasional major shower peak to be practical for many years"*. Other than during major meteor shower maxima, the capture of fireball images is still very much down to chance-capture during imaging of other objects.

Much is about to change, however, as we will read in the final part of this series of articles ...

References

Bone N. M. (2007). "Kappa Cygnid meteor 2007 August 12". *The Astronomer*, **44:521**, C3. [Cover 19].

Fischer D. and McBeath A. (2006). "Responses to 'Meteor Observing in the 21st Century'". *The Astronomer*, **43:506**, 45–46. [45-46].

Hurst G. M. (2012). "Colin Pillinger and Meteorite in Salisbury Museum". *The Astronomer*, **49:582**, 142. [142].

Markham T. (2010a). "International Meteor Conference held in Armagh 2010 Sep 16-19". *The Astronomer*, **47:558**, 157. [157].

Markham T. (2010b). "Meteor observing: Ageing and limiting magnitudes". *The Astronomer*, **46:550**, 267. [267].

Markham T. (2012a). "2012 International Meteor Conference". *The Astronomer*, **49:582**, 159–160. [159-160].

Markham T. (2012b). "The challenge of observing meteors and fireballs visually (part 1)". *The Astronomer*, **49:578**, 43–44. [43-44].

Markham T. (2012c). "The challenge of observing meteors and fireballs visually (part 2)". *The Astronomer*, **49:579**, 74–75. [74-75].

McBeath A. (2001). "Fireball, Oct 27-28". *The Astronomer*, **38:452**, 213. [6:213].

McBeath A. (2010). "The decline in meteor observing". *The Astronomer*, **47:553**, 15–16.

Meadows P. (2010). "Perseid fireball, 2010 August 11". *The Astronomer*, **47:557**, C1. [Cover 17].

Meadows P. (2011). "Leonid 2011 Nov 19 04h07mUT". *The Astronomer*, **48:572**, C3. [Cover 31].

Meadows P., James N. D., and Ward W. (2011). "Meteor Notes". *The Astronomer*, **48:572**, 213–214. [213-214].

Meadows P., James N. D., and Ward W. (2012). "Meteor Notes". *The Astronomer*, **49:581**, 124–126. [124-126].

Mobberley M. (2001). "Leonid fireball passing through Orion, 2001 Nov 18". *The Astronomer*, **38:452**, C1. [Cover 2:13].

Mobberley M. (2002). "The explorers Leonids 2001 expedition to Palau". *The Astronomer*, **38:454**, 270–273. [6:270-6:273].

Nemiroff R. and Bonnell J. (2003). "Astronomy Picture of the Day: An Unusual Event Over South Wales". https://apod.nasa.gov/apod/ap031001.html .

The Astronomer (2001). "Meteor notes". *The Astronomer*, **38:452**, 213–217. [6:213-6:217].

The Astronomer (2002a). "Meteor notes". *The Astronomer*, **38:453**, 244–246. [6:244-6:246].

The Astronomer (2002b). "Meteor notes". *The Astronomer*, **39:464**, 203–207. [203-207].

The Astronomer (2003). "Meteor notes". *The Astronomer*, **40:475**, 175–176. [175-176].

The Astronomer (2004). "Meteor notes". *The Astronomer*, **41:488**, 204–205. [204-205].

The Astronomer (2005). "Meteor notes". *The Astronomer*, **42:499**, 180. [180].

The Astronomer (2006). "Meteor notes". *The Astronomer*, **43:512**, 204–207. [204-207].

The Astronomer (2007). "Meteor notes". *The Astronomer*, **43:513**, 237–238. [not available].

The Astronomer (2008). "Meteor notes". *The Astronomer*, **44:526**, 267. [267].

The Astronomer (2009a). "Meteor notes". *The Astronomer*, **46:542**, 51. [51].

The Astronomer (2009b). "Meteor notes". *The Astronomer*, **46:543**, 70. [70].

The Astronomer (2009c). "Meteor notes". *The Astronomer*, **46:544**, 103. [103].

The Astronomer (2010). "Meteor notes". *The Astronomer*, **47:556**, 101. [101].

The Astronomer (2011a). "2010 Dec 8 fireball at approx 17:35 UT". *The Astronomer*, **47:561**, 240. [240].

The Astronomer (2011b). "Meteor notes". *The Astronomer*, **48:571**, 185–186. [185-186].

The Astronomer (2012a). "2012 Mar 3, fireball". *The Astronomer*, **48:575**, 296–297. [296-297].

The Astronomer (2012b). "2012 Sep 21 UK fireball". *The Astronomer*, **49:582**, 159. [159].

The Astronomer (2012c). "Meteor notes". *The Astronomer*, **49:577**, 14–16. [14-16].

Ward W. (2006). "Meteor Notes". *The Astronomer*, **43:512**, 205–206. [205-206].

Ward W. (2007). "Sporadic during Perseid watch, 2007 Aug 12". *The Astronomer*, **44:521**, C1. [Cover 17].

Ward W. (2010). "Orionid 2010 Oct 23". *The Astronomer*, **47:559**, C2. [Cover 26].

Back issues of most issues of the magazine have been uploaded to the NASA ADS system and can be downloaded via this link on the magazine's home page: http://www.theastronomer.org/post/NASA%20ADS/

Unfortunately, the page-ids stored in the NASA ADS system don't always directly match the page numbers from the printed magazine. To help mitigate this problem, those page-ids that differ from the printed values have been included (when available) in brackets at the end of each reference.

Handling Editor: Javor Kac

The International Meteor Organization

www.imo.net

Follow us on Facebook InternationalMeteorOrganization

Follow us on Twitter @IMOMeteors

Council

President: Cis Verbeeck,
Bogaertsheide 5, 2560 Kessel, Belgium.
e-mail: cis.verbeeck@scarlet.be

Vice-President: Juraj Tóth,
Fac. Math., Phys. & Inf., Comenius Univ.,
Mlynska dolina, 84248 Bratislava, Slovakia.
e-mail: toth@fmph.uniba.sk

Secretary-General: Robert Lunsford,
14884 Quail Valley Way, El Cajon,
CA 92021-2227, USA. tel. +1 619 755 7791
e-mail: lunro.imo.usa@cox.net

Treasurer: Marc Gyssens, Heerbaan 74,
B-2530 Boechout, Belgium.
e-mail: marc.gyssens@uhasselt.be
BIC: GEBABEBB
IBAN: BE30 0014 7327 5911
Bank transfer costs are always at your expense.

Other Council members:

Megan Argo, Jodrell Bank Centre for Astrophysics,
Alan Turing building, University of Manchester,
Oxford Road, Manchester, M13 9PL, UK.
e-mail: megan.argo@gmail.com

Javor Kac (see details under WGN)

Detlef Koschny, Zeestraat 46,
NL-2211 XH Noordwijkerhout, Netherlands.
e-mail: detlef.koschny@esa.int

Masahiro Koseki, 4-3-5 Annaka, Annaka-shi,
Gunma-ken 379-0116, Japan.
e-mail: geh04301@nifty.ne.jp

Sirko Molau, Abenstalstraße 13b, D-84072 Seysdorf,
Germany. e-mail: sirko@molau.de

Jean-Louis Rault, Société Astronomique de France,
16, rue de la Vallée, 91360 Epinay sur Orge,
France. e-mail: f6agr@orange.fr

Jürgen Rendtel, Eschenweg 16, D-14476 Marquardt,
Germany. e-mail: jrendtel@aip.de

Paul Roggemans, Pijnboomstraat 25, 2800 Mechelen,
Belgium, e-mail: paul.roggemans@gmail.com

Galina Ryabova, Res. Inst. of Appl. Math. & Mech.,
Tomsk State University, Lenin pr. 36, build. 27,
634050 Tomsk, Russian Federation.
e-mail: ryabova@niipmm.tsu.ru

Damir Šegon, J. Rakovca 3, 52100 Pula, Croatia.
e-mail: damir.segon@pu.t-com.hr

Commission Directors

Visual Commission: Rainer Arlt (rarlt@aip.de)
Generic e-mail address: visual@imo.net
Electronic visual report form:
http://www.imo.net/visual/report/electronic

Video Commission: Sirko Molau (video@imo.net)

Photographic Commission: Bill Ward
(William.Ward@glasgow.ac.uk)
Generic e-mail address: photo@imo.net

Radio Commission: Jean-Louis Rault (radio@imo.net)

Fireballs: Online fireball reports:
http://fireballs.imo.net

Outreach Officer

Jure Atanackov, e-mail: jureatanackov@gmail.com

Webmaster

Karl Antier, e-mail: webmaster@imo.net

WGN

Editor-in-chief: Javor Kac
Na Ajdov hrib 24, SI-2310 Slovenska Bistrica,
Slovenia. e-mail: wgn@imo.net;
include METEOR in the e-mail subject line

Editorial board: Ž. Andreić, M. Argo, D.J. Asher,
F. Bettonvil, J. Correira, M. Gyssens,
C. Hergenrother, T. Heywood, J.-L. Rault,
J. Rendtel, C. Verbeeck, S. de Vet, D. Vida.

IMO Sales

Available from the Treasurer or the Electronic Shop on the IMO Website	€	$
IMO membership, including subscription to WGN Vol. 47 (2019)		
Surface mail	26	32
Air Mail (outside Europe only)	49	60
Electronic subscription only	21	25
Proceedings of the International Meteor Conference on paper		
1990, 1991, 1993, 1995, 1996, 1999, 2000, 2002, 2003, per year	9	12
2007, 2010, 2011, per year	15	20
2012, 2013, 2014, 2015 per year	25	34
Proceedings of the Meteor Orbit Determination Workshop 2006	15	20
Radio Meteor School Proceedings 2005	15	20
Handbook for Meteor Observers	15	20
Meteor Shower Workbook	12	16
Electronic media		
Meteor Beliefs Project ZIP archive	6	8

Bright fireball of 2018 September 11 over Slovenia

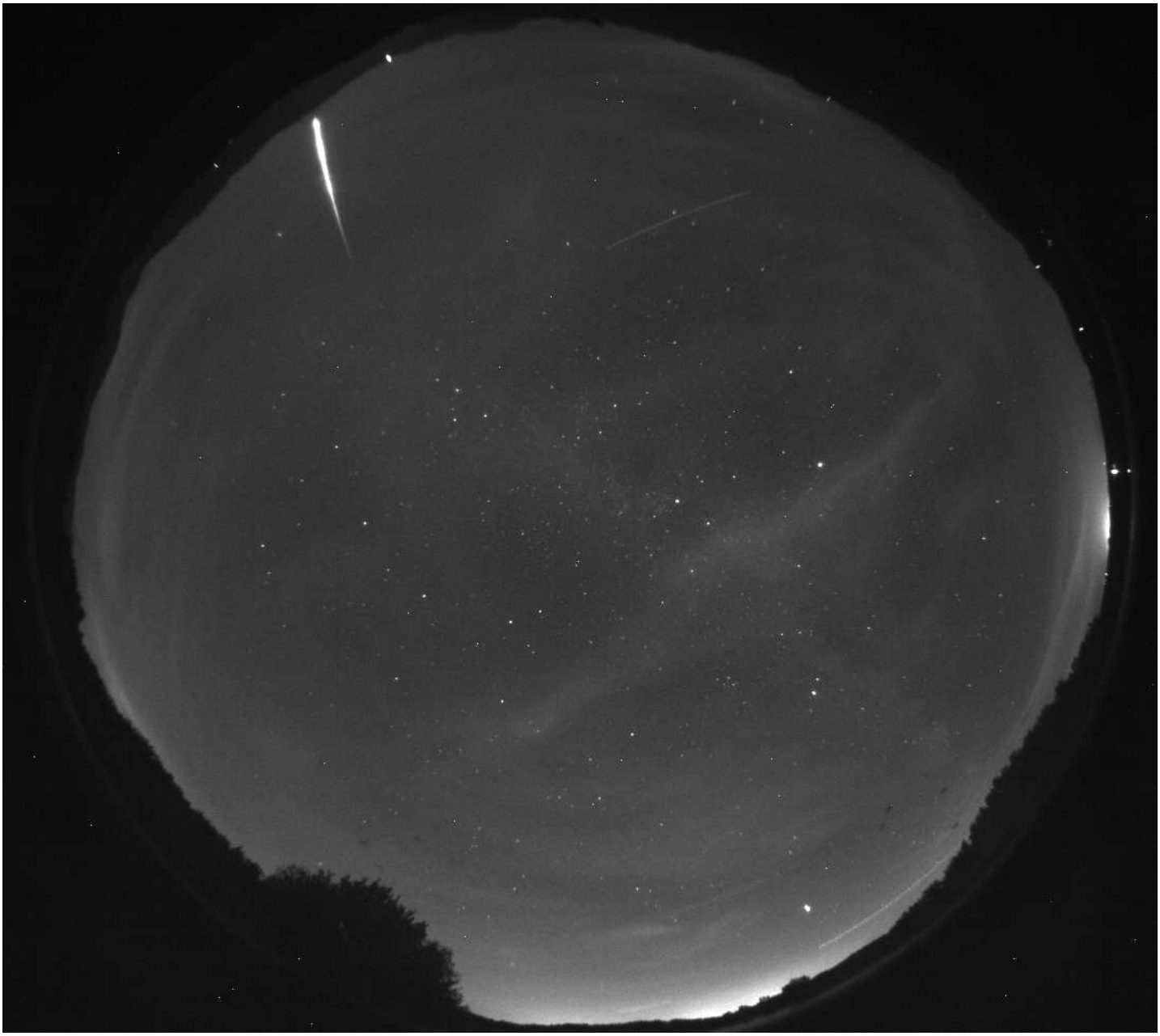

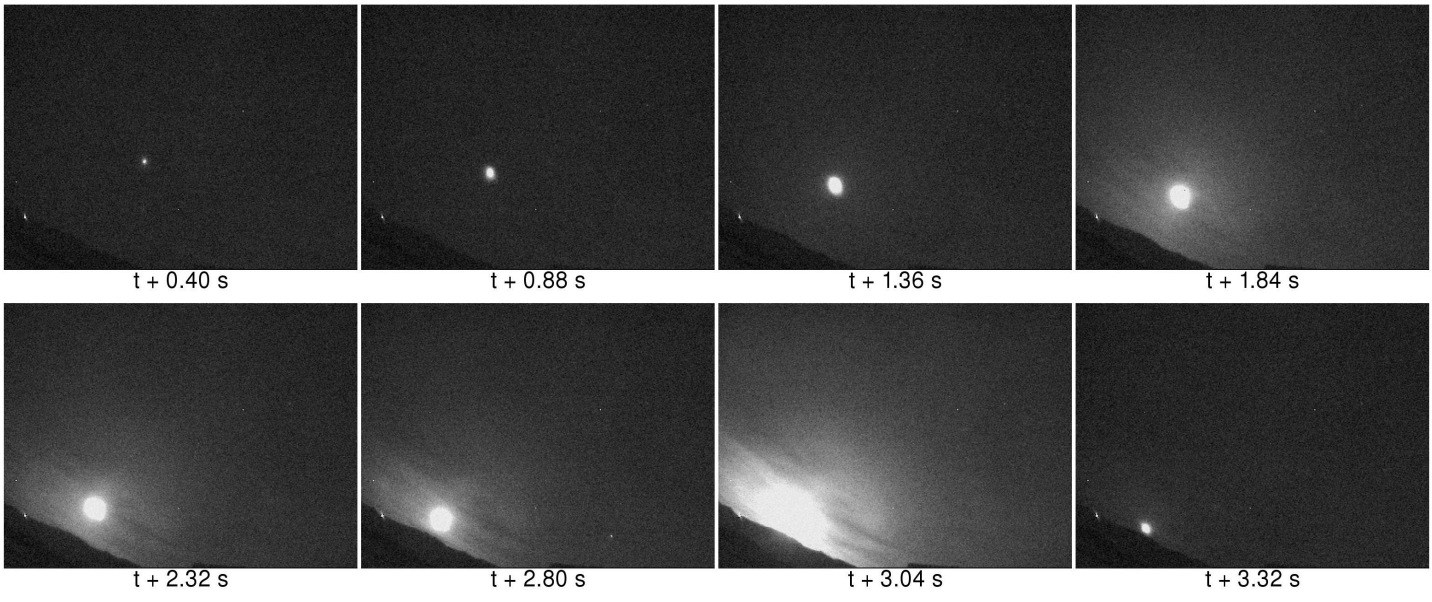

This bright fireball was recorded on 2018 September 11 at $21^{\mathrm{h}}46^{\mathrm{m}}47^{\mathrm{s}}$ by the Rezman Observatory all-sky camera (top) and video camera Cvetka (bottom). Frames are marked with time since the beginning of the fireball. Photo courtesy: Javor Kac/Rezman Observatory.